การศึกษาคุณลักษณะและความว่องไวในการเร่งปฏิกิริยาด้วยแสง ของอนุภาคซิงค์ออกไซด์ที่เตรียมด้วยวิธีอาร์คดิสชาร์จ

นางสาวช่อทิพย์ เติมพรวิทิต

วิทยานิพนธ์นี้เป็นส่วนหนึ่งของการศึกษาตามหลักสูตรปริญญาวิศวกรรมศาสตรมหาบัณฑิต
สาขาวิชาวิศวกรรมเคมี ภาควิชาวิศวกรรมเคมี
คณะวิศวกรรมศาสตร์ จุฬาลงกรณ์มหาวิทยาลัย
ปีการศึกษา 2556

CHARACTERIZATIONS AND PHOTOCATALYTIC ACTIVITY OF ZINC OXIDE NANOPARTICLES PREPARED BY ARC DISCHARGE

Ms. Chortip Termpornvithit

A Thesis Submitted in Partial Fulfillment of the Requirements
for the Degree of Master of Engineering Program in Chemical Engineering
Department of Chemical Engineering
Faculty of Engineering
Chulalongkorn University
Academic Year 2013

Thesis Title	CHARACTERIZATIONS AND PHOTOCATALYTIC ACTIVITY OF ZINC OXIDE NANOPARTICLES PREPARED BY ARC DISCHARGE
By	Ms. Chortip Termpornvithit
Field of Study	Chemical Engineering
Thesis Advisor	Assistant Professor Varong Pavarajarn, Ph.D.

Accepted by the Faculty of Engineering, Chulalongkorn University in Partial Fulfillment of the Requirements for the Master's Degree

…….… Dean of the Faculty of Engineering
(Professor Bundhit Eua-Arporn, Ph.D.)

THESIS COMMITTEE

..... Chairman
(Professor Sutthichai Assabumrungrat, Ph.D.)

..... Thesis Advisor
(Assistant Professor Varong Pavarajarn, Ph.D.)

……..... Examiner
(Assistant Professor Apinan Soottitantawat, D.Eng.)

……..... External Examiner
(Busarakam Charnhattakorn, D.Eng.)

ช่อทิพย์ เติมพรวิทิต : การศึกษาคุณลักษณะและความว่องไวในการเร่งปฏิกิริยาด้วยแสงของอนุภาคซิงค์ออกไซด์ที่เตรียมด้วยวิธีอาร์คดิสชาร์จ (CHARACTERIZATIONS AND PHOTOCATALYTIC ACTIVITY OF ZINC NANOPARTICLES BY ARC DISCHARGE) อ. ที่ปรึกษาวิทยานิพนธ์หลัก: ผศ.ดร.วรงค์ ปวราจารย์, 78 หน้า.

งานวิจัยนี้สามารถสังเคราะห์อนุภาคซิงค์ออกไซด์ขนาดนาโนด้วยวิธีอาร์คดิสชาร์จในน้ำจากการใช้ขั้วไฟฟ้าที่แตกต่างกันโดยจัดให้แท่งสังกะสีเป็นขั้วแอโนดในขณะที่แท่งแกรไฟต์เป็นแคโทดได้เป็นผลสำเร็จ การอาร์คเกิดขึ้นเมื่อก๊าซผสมระหว่างออกซิเจนและไนโตรเจนถูกป้อนเข้าสู่ระบบผ่านช่องว่างในขั้วแคโทดพร้อมกันกับการจ่ายกระแสไฟฟ้า ส่งผลให้สังกะสีที่ขั้วแอโนดระเหยกลายเป็นไอทำปฏิกิริยากับก๊าซออกซิเจนที่ป้อนเข้ามาเกิดการก่อตัวเป็นอนุภาคซิงค์ออกไซด์ ในการสังเคราะห์อนุภาคซิงค์ออกไซด์นี้ได้ศึกษาผลกระทบของความเร็วในการเคลื่อนที่ของขั้วแอโนด กระแสไฟฟ้าที่ใช้ในการจ่ายเข้าสู่ระบบ อุณหภูมิของน้ำ รวมไปถึงอัตราส่วนของก๊าซออกซิเจนในก๊าซผสม ผลจากกล้องจุลทรรศน์แบบส่องกราดแสดงให้เห็นว่าอนุภาคซิงค์ออกไซด์ที่สังเคราะห์ได้มีลักษณะเป็นกึ่งทรงกลมและวงรีโดยมีขนาดอยู่ระหว่าง 20-50 นาโนเมตร จากการศึกษาสมบัติทางแสงของผลิตภัณฑ์ที่ได้ชี้ให้เห็นว่าอนุภาคมีการปล่อยพลังงานออกมาในช่วงของแสงสีฟ้าซึ่งแสดงถึงความไม่สมบูรณ์ของผลึกจากการมีสังกะสีส่วนเกิน ส่งผลให้ขนาดช่องว่างพลังงานของอนุภาคซิงค์ออกไซด์ลดลง นอกจากนี้การศึกษาความว่องไวในการเร่งปฏิกิริยาด้วยแสงของอนุภาคซิงค์ออกไซด์โดยประเมินผลจากการสลายตัวของเมทิลีนบลูพบว่าความไม่สมบูรณ์ของผลึกจากการมีซิงค์เกินบนพื้นผิวของอนุภาคซิงค์ออกไซด์ส่งผลต่อประสิทธิภาพของผลิตภัณฑ์ในการนำไปใช้เป็นตัวเร่งของปฏิกิริยาสลายตัวของเมทิลีนบลูได้เช่นเดียวกันกับขนาดและพื้นที่ผิว

ภาควิชา วิศวกรรมเคมี ลายมือชื่อนิสิต .....

สาขาวิชา วิศวกรรมเคมี ลายมือชื่อ อ.ที่ปรึกษาวิทยานิพนธ์หลัก .....

ปีการศึกษา 2556

5470165121: MAJOR CHEMICAL ENGINEERING
KEYWORDS : ZINC OXIDE NANOPARTICLES/ARC DISCHARGE/ PHOTOCATALYTIC ACTIVITY/ZINC INTERSTITIAL DEFECT

CHORTIP TERMPORNVITHIT: CHARACTERIZATIONS AND PHOTOCATALYTIC ACTIVITY OF ZINC NANOPARTICLES BY ARC DISCHARGE. ADVISOR: ASST. PROF. VARONG PAVARAJARN, Ph.D., 78 pp.

ZnO nanoparticles were successfully synthesized by arc discharge using two difference electrodes, i.e., a zinc anode and a graphite cathode, which were submerged in de-ionized water. Gas mixture of oxygen and nitrogen was continuously supplied through holes in the cathode, while the arc was initiated by applying electrical current between the electrodes. Consequently, zinc anode was vaporized and reacted with oxygen to form ZnO nanoparticles. The effects of synthesis parameters, which are anode speed, arc current, water temperature and oxygen concentration in the gas mixtures on characteristics of ZnO nanoparticles were investigated and reported. Electron microscopy showed that the products are semispherical and ellipsoid particles with the average size of 20-50 nm. Optical characterizations indicated blue photoluminescence emission which corresponds to Zn interstitial defects of ZnO and leads to reduction in the band gap of the products. The photocatalytic activity of the as-prepared ZnO nanoparticles was evaluated via methylene blue (MB) degradation. The results showed that not only the particle size and surface area affects photocatalytic activity of the synthesized ZnO but also the intrinsic defect on the surface.

Department : Chemical Engineering Student's Signature .....
Field of Study : Chemical Engineering Advisor's Signature .....
Academic Year : 2013

ACKNOWLEDGEMENTS

The author would like to express her sincere gratitude to her thesis advisor, Asst. Prof. Prof. Varong Pavarajarn, Department of Chemical Engineering, Chulalongkorn University for his helpful, invaluable suggestion, deep discussion and encouragement to pass by the problems and obstacles throughout the course of this work.

Furthermore, the author would like to express special thanks to Assistant Professor Apinan Soottitantawat, Ph. D., Department of Chemical Engineering, Faculty of Engineering, Chulalongkorn University and Busarakam Charnhattakorn, D. Eng., for their useful comments and participation as the thesis committee.

In addition, the author wishes to thank the member of the Center of Excellence in Particle technology, Department of Chemical Engineering, Faculty of Engineering, Chulalongkorn University for their suggestion, assistance and warm collaboration.

Finally, the author would like to deep thank and appreciate to her parent who always loves, supports, advices, and be her motivation throughout the course of her life.

CONTENTS

Page

CHAPTER **Page**

CHAPTER **Page**

CHAPTER **Page**

LIST OF TABLES

LIST OF FIGURES

Figure **Page**

Figure **Page**

Figure **Page**

CHAPTER I

INTRODUCTION

Pollution crisis has always been a major problem throughout the world especially in the developing country. Among many pollution problems, the water pollution is considered as a serious consequence which contributes to the effect in human health, plants and animal ecosystems. It can be generated from domestic, agricultural and also industrial activities from which organic pollutants are introduced into the environment. Hence, many practical solutions for minimizing the present level of the organic pollutant from wastewater were examined. One of the effective methods is the photodegradation of organic compounds using a photocatalyst.

Zinc oxide (ZnO), a wide direct band gap (3.37 eV) semiconductor with large exciton binding energy of 60 meV, has received intensive scientific attention because of its unique properties and applications in photocatalysis, electronic nano-devices, ultraviolet (UV) light emitters, piezoelectric nano-generators, chemical sensors and biodevices [1]. Specially, much attention has been drawn towards photocatalytic properties of ZnO. Several researches in recent years have shown that ZnO nanoparticles can be used as a photocatalyst for the degradation of organic pollutants from water and the sterilization of pernicious bacteria and viruses [2-4]. Moreover, it has been proven to be an appropriate alternative to TiO_2 since their mechanisms for photodegradation are similar and sometimes ZnO has been reported to be more efficient than TiO_2 [5].

In a photocatalytic system, photo-induced molecular transformations or reactions occur at the interface between surface of the catalyst and organic pollutants. The morphology and crystal size of catalyst which affects surface atomic arrangements and coordination play an important role in this system [6, 7]. The requirements to improve the photocatalytic activity include the increase in the specific surface area and enhancement of the crystallinity of the catalyst. Consequently, large effort has been focused on the synthesis of ZnO nanoparticles which is used as catalyst for photodegradation [2-4, 8].

Various methods have been used to prepare ZnO nanoparticles such as chemical vapor deposition (CVD), electrochemical deposition, thermal evaporation and sol–gel [6-9]. However, most methods as previously mentioned require high temperature, complicated procedures, special conditions and high-cost experiment. Thus, the electrical arc discharge in liquid is considered in this research because of simplicity to set up experiment, less steps of production, no need for complicated equipments and high yield of nanoparticles products.

The electrical arc discharge process in liquid has been used to synthesize carbonaceous nanostructures such as multi-wall carbon nanotubes, single-wall carbon nanotubes, single-wall carbon nanohorns and nano-onions [10]. Few papers have published the synthesis of metal and metal oxide nanostructures by arc discharge. In recent years, the effect of arc current on size distribution and the photocatalytic activity of the ZnO nanostructures produced by arc discharge method in DI water have been studied using zinc wire as cathode and anode [11].

In this research, the inexpensive and one-step synthesis method by arc discharge in liquid with different electrodes will be used for synthesis of ZnO nanoparticles. Greater extent in synthesis conditions will be investigated to study morphology, size distribution and photocatalytic activity of the produced nanoparticles.

Objectives of the research are listed as following:

1. To synthesize zinc oxide nanoparticles via arc discharge process.
2. To study the effects of parameters used to produce fine zinc oxide particles.
3. To investigate the photocatalytic activity of the produced nanoparticles.

The research is consisted of five chapters as following:

Chapter I suggests the motivation and introduction of this work.

Chapter II describes the theory and previous works relating to synthesis of ZnO nanoparticles, chemical and physical properties of zinc oxide, principal of arc discharge process, synthesis of nanomaterials by arc discharge process, photocatalysis reaction and kinetics of photodegradation.

Chapter III presents materials, apparatus, experimental procedure and characterization of product.

Chapter IV describes the results and discussion of the research.

Chapter V, the last chapter, concludes the overall results of this research and recommendations for future work.

CHAPTER II

THEORY AND LITERATURE REVIEWS

This chapter describes theory and literature reviews relating to properties and synthesis of zinc oxide, principal of arc discharge process and synthesis of nanomaterials by arc discharge process. Furthermore, the photocatalysis reaction will also be explained.

2.1 Physical and Chemical Properties of Zinc Oxide

Zinc oxide which has a formula of ZnO is an inorganic compound. It is generally a white powder. It can be soluble in most acids, ammonia, ammonium carbonate, fixed alkali and hydroxide solution but nearly insoluble in water. It occurs in nature as mineral zincite, however most ZnO is synthetically produced in industrial scale through the oxidation of vaporized zinc metal with preheated air. The basic properties of wurtzite ZnO are represented in Table 2.1 [12].

Table 2.1 Properties of wurtzite zinc oxide.

Molecular formula	ZnO
Molecular weight	81.38 g/mol
Density	5.606 g/cm^3
Melting point	1975 ^{o}C
Thermal conductivity	130 W/m.K
Static dielectric constant	8.656
Energy gap	3.37 eV (direct band gap)
Excitation binding energy	60 meV
Lattice parameters at 300 K	
a	0.32495 nm
c	0.52069 nm
a/c	1.602 (ideal hexagonal structure is 1.633)

In the normal form, ZnO is an n-type semiconductor which has a relatively large direct band gap of 3.37 eV at room temperature. It exhibits excellent piezoelectric, optical properties and stability. Furthermore, it has been proposed to be a UV emitting phosphor because of its larger exciton binding energy (60 meV) which leads to a reduced UV lasing threshold and yields higher UV emitting efficiency at room temperature [13].

ZnO powder is widely used in numerous industrial applications. It is used as a functional material in plastics, cosmetics, ceramics, glass, pigments, paints and etc. It is also used as antiseptic and astringent in pharmaceutical industry. It is also useful in biochemical activity for the preservation of plantation latex. Moreover, for the electronic applications, it can be used as a thin layer for surface acoustic wave devices due to a non-center-symmetric structure of the tetrahedral coordination in ZnO crystals. Other applications can be in air or liquid vibration sensors, transparent transistors, solar cells and memory devices [14-16].

2.2 Crystal Structure and Lattice Parameters of Zinc Oxide

The two main forms of crystalline structure of ZnO are hexagonal wurtzite and cubic zincblende as shown in Figure 2.1 (a) and (b), respectively. Another crystalline structure of zinc oxide is the rocksalt as shown in Figure 2.1 (c). However, ZnO crystals are most commonly stabilized in the hexagonal wurtzite structure whereas the zincblende form can be stabilized only by growing ZnO on cubic substrates. For the rocksalt phase, it can be crystallized at high pressure but cannot be epitaxially stabilized.

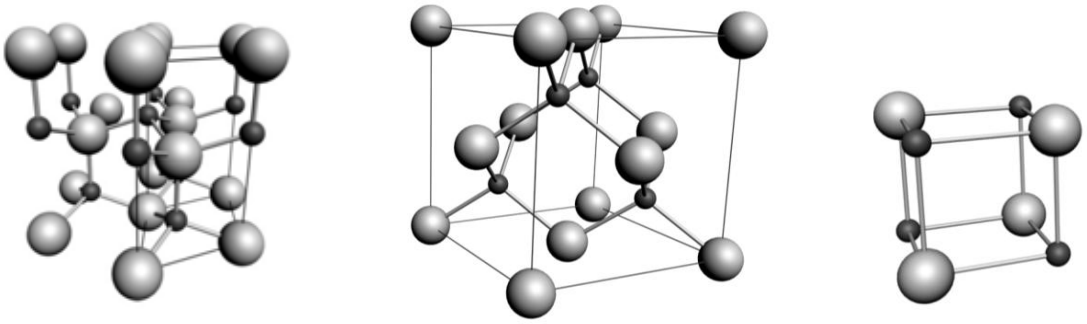

(a) (b) (c)

Figure 2.1 Schematic structures of ZnO using the ball-and-stick model show (a) hexagonal wurtzite, (b) cubic zincblende and (c) cubic rocksalt. Gray large spheres and black spheres denote O and Zn atoms, respectively [17].

ZnO crystal in the wurtzite structure is composed of two interpenetrating hexagonal-close-packed (hcp) sublattices of Zn^{2+} and O^{2-} at which each Zn ion is surrounded by a tetrahedral of O ions. The tetrahedral coordination gives rise to polar symmetry along the hexagonal axis. This polarity is responsible for piezoelectricity, number of the properties of ZnO and spontaneous polarization. In addition, it is also a key factor in etching, crystal growth and defect generation. The four most common face terminations of wurtzite ZnO are the polar Zn terminated (0001) and O terminated $(000\bar{\bar{1}})$ faces (*c*-axis oriented), and the non-polar $(11\bar{2}0)$ (*a*-axis) and $(10\bar{1}0)$ faces which both of which contain an equal number of Zn and O atoms. The polar faces are known to posses different chemical and physical properties and the O-terminated face possesses a slightly different electronic structure to the other three faces. The most common surface is the basal plane (0001). Moreover, the polar surfaces and the $(10\bar{1}0)$ surface are found to be stable, while the $(11\bar{2}0)$ face is less stable and generally has a higher level of surface roughness than its counterparts.

Wurtzite zinc oxide has lattice parameters of a = 3.2495Å and c = 5.2069 Å, and the density of 5.605 g cm^{-3}. A detailed schematic representation of the wurtzite ZnO lattice structure is shown in Fig. 2.2. In an ideal wurtzite crystal, the axial ratio c/a and the u parameter (which is a measure of the amount by which each atom is

displaced with respect to the next along the *c*-axis) are correlated by the relationship $uc/a = (3/8)^{1/2}$, where $c/a = (8/3)^{1/2}$ and $u = 3/8$ for an ideal crystal. Experimentally, the real values for wurtzite ZnO of u and c/a were determined in the range $u = 0.3817–0.3856$ and $c/a = 1.593–1.6035$.

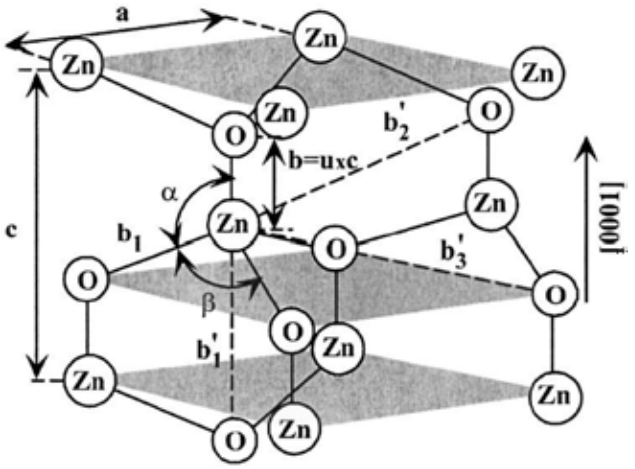

Figure 2.2 Schematic lattice structure of a wurtzite ZnO having constants *a* in the basal plane and *c* in the basal direction; *u* parameter is expressed as the bond length or the nearest-neighbor distance *b* divided by *c* 0.375 in ideal crystal, and α and β (109.47° in ideal crystal) are the bond angles[18].

2.3 Typical Growth of Zinc Oxide

ZnO basically has three types of fast growth directions: ⟨ 2110 ⟩ (i.e., ±[2110], ±[1210], ±[1120]); ⟨ 0110 ⟩ (i.e., ±[0110], ±[1010], ±[1100] and ±[0001]. ZnO exhibits a wide range of novel structures which can be grown by tuning the growth rates along these directions together with the polar surfaces due to atomic terminations. The relative surface activity of various growth facets is one of the most profound factors for determining the morphology under given conditions.

Macroscopically, a crystal has different kinetic parameters for different crystal planes, which are emphasized under controlled growth conditions. Thus, after an initial period of nucleation and incubation, a crystallite will commonly develop into a

three dimensional object with well-defined, low index crystallographic faces. Figure 2.3 shows typical growth morphologies of one dimensional nanostructure for ZnO.

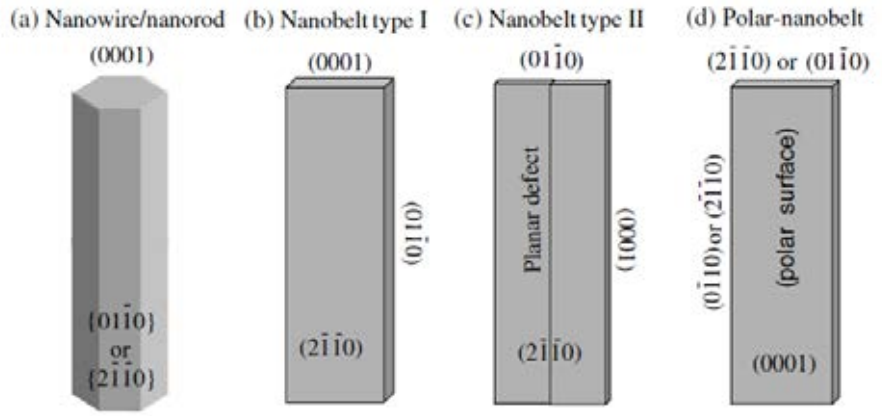

Figure 2.3 Typical growth morphologies of one-dimensional ZnO nanostructures and the corresponding facets[14].

These structures tend to maximize the area of the { 2110 } and { 0110 } facets because they have lower energy. The different surface structures of ZnO could induce anisotropic growth. The morphology shown in Figure 2.3 is dominated by the polar surfaces, which can be grown by introducing planar defects parallel to the polar surfaces. Planar defects and twins are observed occasionally parallel to the (0001) plane, but dislocations are rarely seen.

2.4 Point Defect in Zinc oxide

2.4.1 Native Defect

Native or intrinsic defects are imperfections in the crystal lattice that involve only the constituent elements. Vacancies (missing atoms at regular lattice positions), interstitials (extra atoms occupying interstices in the lattice) and antisites (a Zn atom occupying an O lattice site or vice versa) are also considered to be the native defects. They can strongly influence the electrical and optical properties of a semiconductor, affecting doping and luminescence efficiency. In addition, they are

directly involved in the diffusion mechanisms connected to growth, processing and device degradation.

In principle, there are a number of intrinsic defects with different ionization energies. The Kröger Vink notation uses: i = interstitial site, Zn = zinc, O = oxygen, and V = vacancy. The terms indicate the atomic sites, and superscripted terms indicate charges, where a dot indicates positive charge, a prime indicates negative charge, and a cross indicates zero charge, with the charges in proportion to the number of symbols. The donor defects are:Zn_i , $Zn_i^{\bullet}$, Zn_i^{x}, $V_o^{\bullet\bullet}$, $V_o^{\bullet}$, V_o and the acceptor defects are: V_{Zn}, V_{Zn}.

Zn interstitials and oxygen vacancies are known to be the predominant ionic defect types. However, which defect dominates in undoped ZnO is still a matter of great controversy. Zn interstitials and oxygen vacancies come from the Frenkel reaction and the Schottky reaction, repectively[19].

Zn interstitials come from the Frenkel reaction:

$$Zn_{Zn} \Leftrightarrow Zn_i^{x} + V_{Zn}^{x} \qquad (2.1)$$

Further ionization reactions and equilibrium constants are:

$$Zn_i^{x} \Leftrightarrow Zn_i^{\bullet} + e' \qquad \text{K} = 2\text{N}_c \exp(-0.05/\text{kT}) \qquad (2.2)$$

$$Zn_i^{\bullet} \Leftrightarrow Zn_i^{\bullet\bullet} + e' \qquad \text{K} = 1/2\text{N}_c \exp(-0.15/\text{kT}) \qquad (2.3)$$

The oxygen vacancies arise from the Schottky reaction:

$$O \Leftrightarrow V_{Zn}^{x} + V_o^{x} \qquad (2.4)$$

Further ionization reactions and equilibrium constants are:

$$V_o^{x} \Leftrightarrow V_o^{\bullet} + e' \qquad \text{K} = 2\text{N}_c \exp(-0.05/\text{kT}) \qquad (2.5)$$

$$V_o^{\bullet} \Leftrightarrow V_o^{\bullet\bullet} + e' \qquad \text{K} = 1/2\text{N}_c \exp(-2.0/\text{kT}) \qquad (2.6)$$

$$V_{Zn}^{x} \Leftrightarrow V_{Zn}' + h^{\bullet} \qquad \text{K} = 1\ 2\text{NV} \exp(-2.8/\text{kT}) \qquad (2.7)$$

$$V_{Zn}' \Leftrightarrow V_{Zn}'' + h^{\bullet} \qquad \text{K} = 1\ 2\text{NV} \exp(-2.8/\text{kT}) \qquad (2.8)$$

From these defect reactions as shown in Eq. 2.1 to 2.8, it can be seen that the both kinds of defects donate two electrons, and thus it is difficult to distinguish one from the other using electrical measurements.

2.4.2 Oxygen Vacancies

The oxygen vacancies (V_o) is devoted special attention for the visible emission of ZnO. It is a lattice imperfection where one oxygen ion is removed. It can occur in three charged states: the doubly ionized oxygen vacancy($V_o^{\bullet\bullet}$), the singly ionized oxygen vacancy ($V_o^{\bullet}$) and the neutral oxygen vacancy (V_o^{x}). $V_o^{\bullet\bullet}$ is doubly positive charged relative to the lattice of ZnO which does not capture any electrons. $V_o^{\bullet}$ is singly positive charged relative to the lattice which has captured one electron. $V_o^{\bullet}$ is neutral relative to the lattice which has captured two electrons. In the neutral charge state, the four Zn nearest neighbors are displaced inward by 12% of the equilibrium Zn–O bond length. In the single positive charge state, the four Zn nearest neighbors are displaced outward by 3%, and for the double positive charge state the displacements are outward by 23% as shown in figure 2.6 [20].

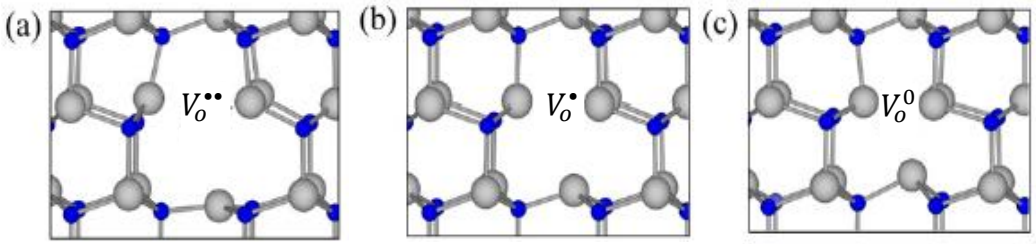

Figure 2.4 Ball and stick model of the local atomic relaxations around the oxygen vacancy in difference charge states.

According to the levels of these three oxygen vacancies in the energy band of ZnO as shown in Figure 2.7, the origin of the yellow, green, and blue peaks can be attributed to the recombination of the $V_o^{\bullet\bullet}$ trapped center with delocalized electrons close to the conduction band, the electron transition from $V_o^{\bullet}$centers to the valence band edge, and electron transition from V_o^{x}centers to valence band edge, respectively [21].

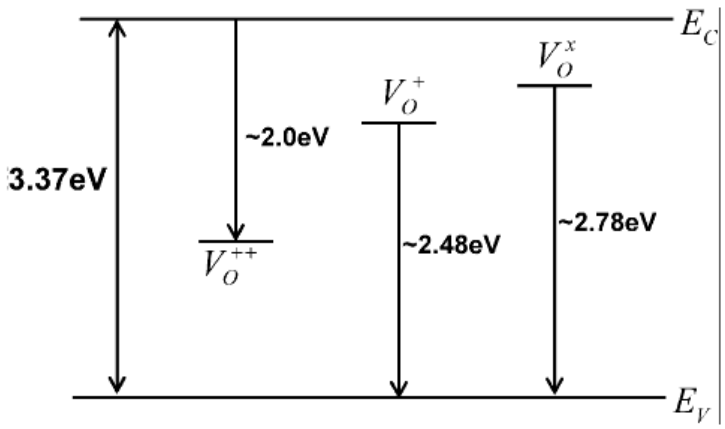

Figure 2.5 Visible radiative emissions of oxygen vacancies of ZnO.

2.4.3 Zn Interstitial

A Zn interstitial atom (Zn_i) could in principle occupy the tetrahedral site or the octahedral site in the ZnO wurtzite structure. At the tetrahedral site, the Zn_i has one Zn and one O as nearest-neighbor atoms at a distance of ~$0.833d_0$ (d_0 is the Zn–O bond length along the *c* axis). At the octahedral site, the Zn_i has three Zn and three O atoms as nearest neighbors at a distance of ~$1.07d_0$. Based on size considerations, it is therefore expected that the Zn interstitial will be more stable at the octahedral site where the geometrical constraints are less severe. Indeed it has been found that the octahedral site is the stable site for Zn_i, whereas the Zn_i at the tetrahedral site is unstable as it spontaneously relaxes to the octahedral site. Regarding its electronic structure, Zn_i induces an a_1 state with two electrons above the conduction band minimum (CBM). These two electrons are transferred to conduction-band states, stabilizing the +2 charge state (Zn_i^{2+}). Hence, Zn_i will always donate electrons to the conduction band, thus acting as a shallow donor.

For the energy level of Zn interstitial in ZnO nanostructures, the emission bands of violet and blue peak are observed (see Figure 2.8). The violet emission band in the visible region is attributed to electronic transition from Zn_i level to the top of the valence band, whereas the blue emission band in the visible region (462 nm) is due to electronic transition from the Zn_i level to the zinc vacancy (V_{Zn}) level.

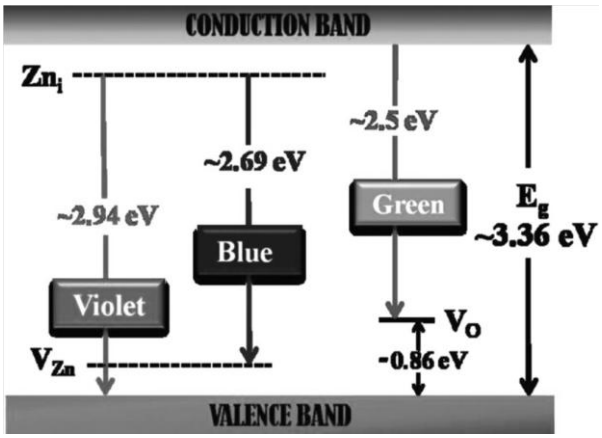

Figure 2.6 Schematic band diagram of the zinc interstitial level of ZnO[22].

2.4.4 Photoluminescence Mechanism of Semiconductor Nanomaterials

A semiconductor is characterized by an electronic band structure in which the highest occupied energy band, called valence band (VB), and the lowest-occupied energy band, called conduction band (CB), are separated by a band gap, i.e. a region of forbidden energies. There are some sub-bands in the band gap, which are closely related to surface defects and surface states. The band gap energy (Eg) is the energy difference between the CB bottom and VB top.

The PL phenomena of excited energy higher or equal to the band gap energy of semiconductor are presented to discuss the relationships between the PL spectrums. Figure 2.7 shows the main photophysical processes of semiconductors excited by light with no less than the band gap energy which consist of four main processes.

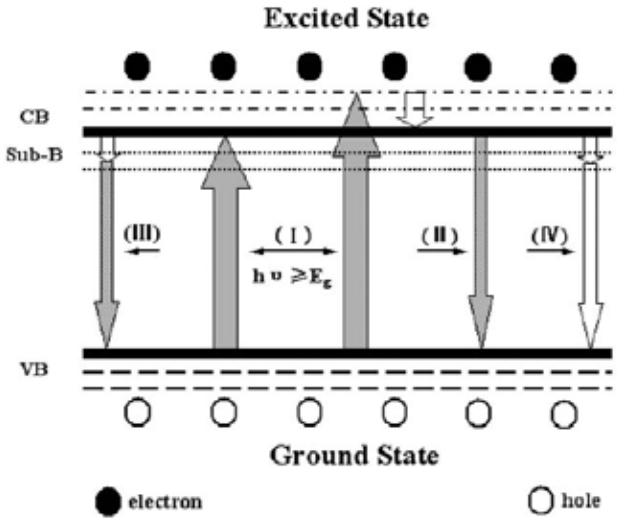

Figure 2.7 Main photophysical processes of a semiconductor excited by light with equal to or higher than band gap energy (I—photo-excited process; II—band–band PL process; III—excitonic PL process; IV—non-radiative transition process) [34].

Process I is the photo-excited process in which the electrons from the VB are promoted to the CB with different energy levels to become different excited states, with simultaneous generation of holes (h+) in the VB under irradiation. However, the excited electrons in the CB easily come back to the VB via a certain course to recombine with the holes, since they are very unstable. During the recombination process of photo-induced charge carriers, a certain amount of chemical energy can be released, which would further transform possibly to heat or to light energy. The light energy can be dissipated as radiation, which results in a luminescence emission of semiconductor material, called the PL phenomenon of the semiconductor. In fact, the excited electrons with different energy levels in the CB easily transfer firstly to the CB bottom via non-radiative transitions; subsequently, the processes II, III or IV will possibly occur. Process II is the band–band PL process in which the electron transitions from the CB bottom to the VB top can take place, with simultaneously releasing of energy as radiation. In this case, the photon energy actually equals to the band gap energy. However, the photon energy can be higher than the band gap energy sometimes, which mainly results from the transitions of higher energy of excited electrons from the CB band to the VB top directly. This PL signal is also attributed to

a kind of band–band PL phenomenon. Process III is the excitonic PL process in which the non-radiative transitions of excited electrons from the CB bottom to different sub bands (or surface states) occur first, and subsequent radiative transitions from the sub-band to the VB top can take place. The energy of the radiative photon, which is the energy difference between the sub-band and VB top, is lower than the band gap energy. In addition, the excited electrons at the CB bottom can come back to the VB directly or indirectly by non-radiative transitions, which is the process IV.

2.5 Arc Discharge Process

Arc discharge or electric arc is the attractive methods to synthesize many kinds of nanomaterials because of the self-crystallization of nanostructures, simplicity of experimental set up, low impurity of the product and low-cost procedure to generate a high yield of products. The early works by this method were based on production of MWCNTs, SWCNTs, SW-CNHs and nano-onions [23-26]. Since then, there have been several researches that have published the synthesis of metal and metal oxide nanoparticles such as Ag, Au, MoS_2, WO_3 and ZnO by using this method [11, 27-29].

2.5.1 Principal Operation of Arc Discharge Process

The principal operation of the arc discharge process will be explained by mean of the synthesis of single-walled carbon nanoparticles using the arc in water with gas injection [25]. The experimental set up is consisted of the reactor including anode and cathode, a high current DC power supply which is used to generate the arc current and the injected gas system. The electrodes are graphite rods which are placed vertically in de-ionized water to generate an arc discharge. N_2 gas flow is introduced for excluding water from the arc zone through two narrow holes of the cathode. The experimental set-up is shown in figure 2.10.

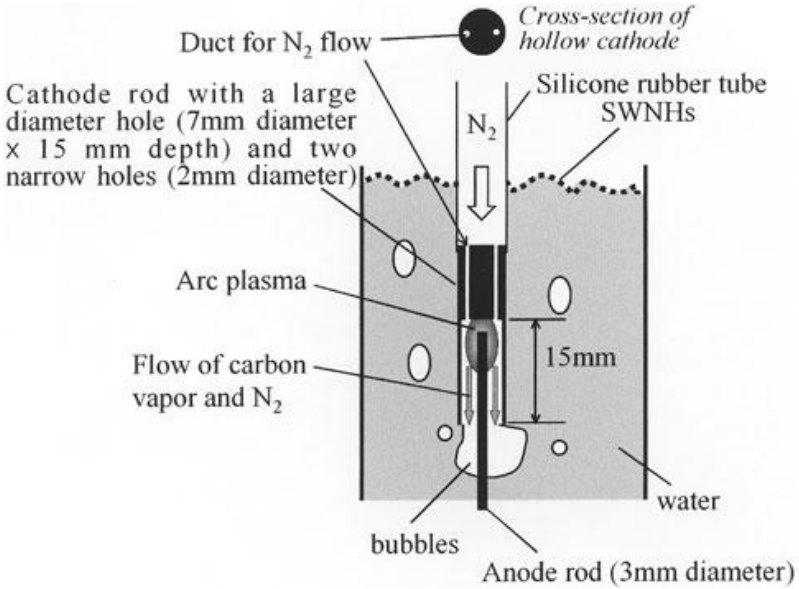

Figure 2.8 Schematic of an arc discharge in water system.

In this set-up, the cathode and anode are connected to the DC power supply, one to the positive pole and the other one to the negative pole. The voltage and the current of the arc discharge are 30–50 V and 30–80 A, respectively. The arc discharge is generated when an electric current passes between the electrodes in the hole of the cathode which is separated into 3 parts, i.e. arcing zone, quenching zone and steaming zone (for arcing in water) [30]. The region in which the reaction took place is called arcing zone and the quenching zone is observed next to the arcing zone. In the steaming zone, water vapor is generated at the liquid-gas interface, resulting in the diffusion of the water vapor toward the quenching zone. When the arc current is supplied to the system, electrons flow from the top of the anode to the cathode and release the energy which leads to evaporation of graphite electrodes. As a result, the anode is evaporated. The N_2 gas flow is served to convey and rapidly quench of the evaporated graphite by its fast transfer from the hot arc spot to cold water and cause self-crystallized nanostructures. During the operation, a thin deposit of approximately 0.5 mm thickness is formed on the inner surface of the cathode hole, and this deposit is continuously peeled away into the water by the arc pressure. Moreover, the fine powders floating on the water surface and at the reactor bottom are obtained.

2.5.2 Synthesis of Nanomaterials by Arc Discharge Process

The arc discharge process was first used by Krastchmer and Hoffman to synthesize C_{60} [31]. In the last two decades, it was widely used to prepare carbon based nanomaterials such as multi-wall carbon nanotubes, single-wall carbon nanotubes, single-wall carbon nanohorns and nano-onions. The synthesis of single-walled carbon nanohorns (SWNHs) by arc discharge between two graphite electrodes submerged in liquid nitrogen was reported. The results indicated that the arc current affects the average particle size of the SWNHs such that increasing of arc current causes the average size to decrease. Furthermore, the particle size distribution is also narrower at higher arc currents [32]. Afterwards, the impact of the gas flow was investigated by synthesized SWCNHs using the arc in water method with the support of N_2 gas injection. It was reported that the flow of N_2 is necessary for SWCNHs formation due to the rapid quenching of the carbon vapor in an inert gas at atmospheric pressure. For further study in products size and their morphology, the various conditions for the synthesis of SWCNHs by a gas-injected arc-in-water have been used. It was revealed that the flow rate, arc current and gas component pay important role for production rate, the yield and specific surface area of the as-grown SWCNHs [33]. Besides, the effect of water temperature was investigated. It showed that the yield of SWCNHs significantly decreases with the increase in water temperature. Nevertheless, the purity of as-grown SWCNHs is not dependent on the temperature change [34].

The metal and metal oxide nanoparticles were also synthesized by the arc discharge process. There are several researches that published the synthesis of metal or metal oxide by using this process. For instance, the silver nanoparticles (AgNPs) were formed by using arc discharge between titanium electrodes in $AgNO_3$ solution instead of using water. The direct reduction of $AgNO_3$ by electrons coming from the discharge zone leads to formation of silver nanoparticles in de-ionized water rather than the use of Ag-electrodes. It was found that sodium citrate acts as a stabilizer and surface capping agent of the nanoparticles. In addition, the quantity of silver nanoparticles was raised by increasing the arc duration [27]. Recently, the synthesis of zinc oxide nanoparticles was fabricated by using high current electrical arc discharge in de-

ionized (DI) water. The zinc rods were used as electrodes for this research. The effect of arc current on nanoparticles size was investigated. The result indicated that the size of ZnO nanoparticles is increases by increasing the arc current [11].

In this research, the arc discharge process in liquid is selected for the synthesis of ZnO. It is expected that the produced particles from this method will be formed in nanosize. The experimental step is the same as that one mentioned in the previous paragraph but the graphite will be used as the cathode while the anode is zinc rod with different diameters. The various conditions will be investigated to study size distribution, morphology and photocalytic activity of produced ZnO by arc discharge process.

2.6 Photocatalytic Process

Photocatalysis is a phenomenon which deals with the oxidation mostly of organic molecules by the use of catalyst which is activated by the incidence of radiation of an appropriate wavelength. It can take place both in the aqueous phase as well as in gas phase. There are two types of photocatalysis which are homogeneous photocatalysis and heterogeneous photocatalysis. In homogeneous photocatalysis, the reactants and the photocatalysts exist in the same phase. For heterogeneous photocatalysis process, the catalyst is in different phase from the reactants. However, heterogeneous photocatalytis has been more described and intensively studied in recent years because of its application in a variety of environmental purification, decomposition of toxic and organic compound [35].

2.6.1 Photocatalytic Reaction

The reaction occurs at the interface between semiconductors, i.e., a solid photocatalyst, and a fluid containing the reactants and products from the reaction. Among several semiconductors, zinc oxide have attracted as promising photocatalysts due to their high photocatalytic activity, resistance to non-toxicity, photocorrosion, photo-stability and low cost. According to process I (photo-excited process) in Figure 2.9, when the semiconductor particle absorbs a photon of light equal to or more

energetic than its band gap width, the electron is excited from the valence band (VB) to the conduction band (CB). Photocatalytic reactions on semiconductor take place and lead to lead to a charge separation due to promotion of an electron (e^-) from the valence band to the conduction band, thus generating a hole (h^+) in the valence band. The schematic of photocatalysis on semiconductor is shown in Figure 2.11 [36].

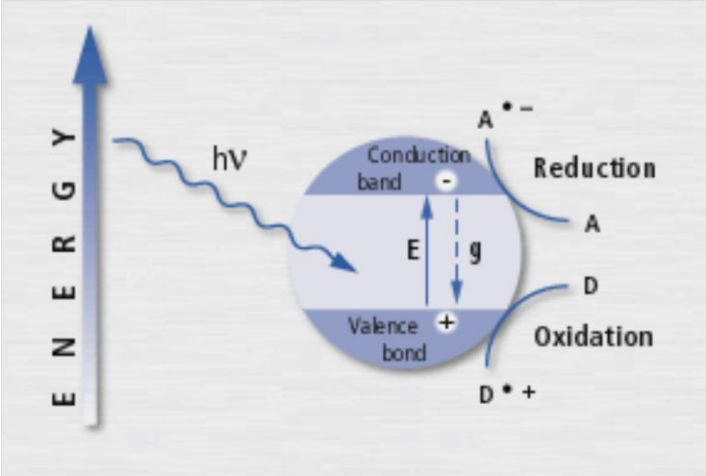

Figure 2.9 The schematic of photocatalysis on semiconductor. VB: valence band, CB: conduction band, A: electronic acceptor compound, D: electronic donating compound.

The generations of electron-hole pairs are represented in Eq. (2.9). At the surface of semiconductor, the oxidation reaction take place by the hole oxidizes hydroxyl group (OH^-) to generate the strong oxidizing hydroxyl radical ($OH^\bullet$). Meanwhile, the electron reduces oxygen to generate the superoxide radical (O_2^-) due to the process is carried out in aerobic conditions as following Eq. (2.10) to (2.12).

$$\text{Semiconductor} + h\nu \rightarrow h^+ + e^- \quad (2.9)$$

$$h^+ + H_2O \xrightarrow[ads]{} OH^\bullet + H^+ \quad (2.10)$$

$$h^+ + OH^- \xrightarrow[ads]{} OH^\bullet \quad (2.11)$$

$$e^- + O_2 \rightarrow O_2^- \quad (2.12)$$

Moreover, the photogenerated holes can oxidize the organic molecule to form R^+. The $OH^\bullet$ radical which is a very strong oxidizing agent can oxidize most organic pollutant to the mineral end-products. Accoeding to this, the reactions at the semiconductor surface causing the degradation of organic pollutant are given in Eq. (2.13) and (2.14),

$$OH^\bullet + \text{Organic} \longrightarrow \text{Degradation products} \quad (2.13)$$

$$h^+ + \text{Organic} \longrightarrow \text{Oxidized products} \quad (2.14)$$

In photocatalysis, the photocatalytic activity (PCA) depends on the ability of the catalyst to create electron–hole pairs, which generate free radicals (hydroxyl radicals: $OH^\bullet$) able to undergo secondary reactions. The resulting free-radicals are very efficient oxidizers of organic matter. Commercial application of the process is called advanced oxidation process (AOP).

Recently, much effort has been devoted to study ZnO as a very promising photocatalyst for photocatalytic degradation of water pollutants. For instance, Mai et al. reported that methyl green (MG) which was simulating textile waste water from associated auxiliary chemicals could be successfully decolorized and degraded by ZnO nanoparticles under visible light irradiation [37]. Besides, Emad et al. achieved complete photodegradation of amoxicillin, ampicillin and cloxacillin antibiotics in aqueous solution under UV light irradiation in the presence of ZnO [38].

Then, the morphologies of inorganic materials are descried to have great effects on their properties and potential applications. It is well known that ZnO exhibits the richest range of morphologies among the wide-band-gap semiconductors. Thus, the study of photocatalytic activity of ZnO nanoparticles has been investigated. Wang et al. reported that ZnO with flower-like morphology was successfully synthesized by a simple low-temperature route in the absence of surfactants. It exhibited improved ability on the photocatalytic degradation of 4-cholrophenol (4-CP) in aqueous solution under UV radiation compared with ZnO nanorods [39]. Another research focused on the specific area which also affects the photocatalytic activity of the photocatalysts. Lei et al. showed a significantly enhanced photocatalytic activity in

the photodegradation of methylene blue (MB) by high specific area of porous ZnO microspheres which is synthesized by precipitation method [40].

However, there are a few researches that pay attention on the photocatalytic activity of ZnO which is synthesized by the arc discharge process. Thus, the study on various conditions that affect the size distribution, defect and photocatalytic activity of ZnO nanoparticles which is synthesized by arc discharge process will be investigated in this research.

2.6.2 *Kinetics of Photocatalytic Degradation*

Considering the degradation rate of the process, initial practical approaches to quantitative description of heterogeneous photocatalysis kinetics has been commonly carried out using a Langmuir-Hinshelwood (L-H) kinetics model. This mathematical model assumes that the reaction occurs on the catalyst surface and the reaction rate (r) is proportional to the fraction of particle surface covered by the pollutant (θ).

$$r = -\frac{dC}{dt} = k_r\theta = k_r \frac{KC}{1+KC} \tag{2.15}$$

Where k_r is the reaction rate constant, K is the constant of adsorption equilibrium, C is the pollutant concentration at any time and t is the irradiation time.

When the solution is highly diluted, the term KC can be neglected. Most of researchers approximated Langmuir – Hinshelwood kinetics to first order kinetics for the condition KC<<1. In this case the reaction is essentially an apparent first order reaction. After integration, Eq. (2.15) can be simplified to Eq. (2.16):

$$\ln \frac{C_0}{C} = k_{app}t \tag{2.16}$$

Where k_{app} is the apparent rate constant of a pseudo first-order reaction.

Recently, the first order rate constants have been used to calculate for the degradation of dye on ZnO. The degradation rate were found to be decrease with an increasing of ZnO particles size [41]. In this work, the effect of size distribution including defect affected on degradation rate of methylene blue was investigated. Kinetics were estimated by monitoring the change in the concentration of methylene blue at certain interval of time. Apparent first order rate constants (k_{app}) were determined by calculating the slope of the obtained line from plot of ln C_o/C versus irradiation time using Eq. 2.16.

CHAPTER III

EXPERIMENTAL

This chapter presents experimental procedure for synthesis and characterization of ZnO. It is consisted of four main parts which are apparatus, synthesis of ZnO by arc discharges process, characterizations of ZnO product and photocatalytic activity measurements.

3.1 Preparation of Zinc Oxide Nanoparticles by Arc Discharge Process

3.1.1 Apparatus

The schematic diagram of the electrical arc discharge process is shown in Figure 3.1.

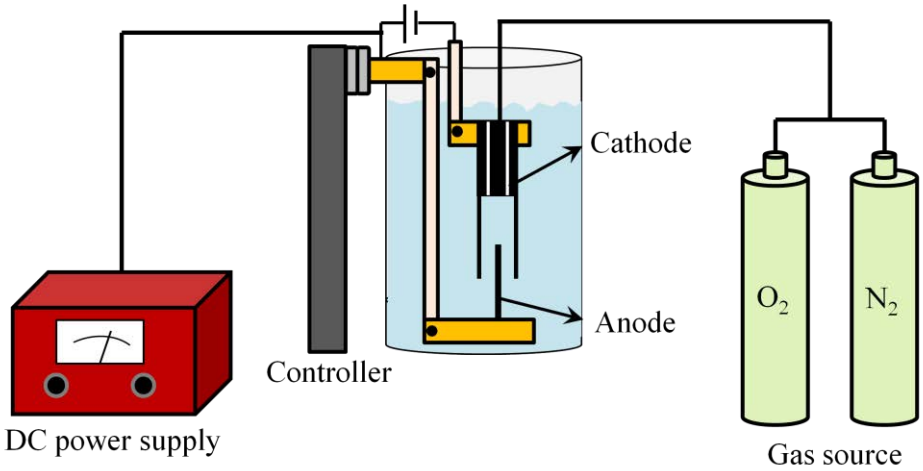

Figure 3.1 Schematic diagram showing the arc discharge process.

In this experiment, two different electrodes are immersed vertically in liquid medium to form an arc discharge system. Zn rod (99.99%, Goodfellow) is used as anode and graphite rod (purity 99.9995%, Alfa Aesar) is used as cathode. It could be note that both anode and cathode should have high conductivity, high corrosion resistance. Moreover, the shape and size must fit in order to carry out its operation.

The anode was 3 mm in diameter. The cathode was 12 mm in diameter with a hole of 8 mm in diameter, 15 mm deep and two narrow holes 1 mm in diameter for supplying gas. The controller, the DC power supply and gas source are set up as shown in above figure. De-ionized water (DI) is used in this experiment as an aqueous media for quenching. The quantity of the liquid used for one batch is about 2000 ml.

3.1.2 Experimental Procedure

The Zn rod and graphite rod were set at the position of anode and cathode, respectively then placed vertically in the liquid. The Zn rod was moved upward into the hole of the graphite rod at controlled speed by a controller. The current is applied between two electrodes by the direct current (DC) power supply. The arc discharge is initiated and the reaction took place when the gap between these two electrodes reached optimum value (about 1-2 mm) to maintain stable discharge. Oxygen (O_2) and nitrogen (N_2) gas were supplied to the system through the narrow holes in the cathode rod to react with the evaporated zinc forming of zinc oxide nanoparticles and then convey from the hot arc spot to cold water. After the arc discharge is terminated, synthesized products suspending in the water including bulk deposits that settling down on the bottom of container will be collected. All products will be dried in an oven at 110 ^{o}C to eliminate the moisture and calcined at 500°C for 2 hours in a box furnace with 10°C/min of the heating rate before characterizations.

3.2 Conditions for Arc Discharge

3.2.1 The Effect of Anode Speed

At first, The effects of anode speed on synthesis of pure ZnO were investigated. The speed was varied at 0.7 mm/s, 1mm/s and 1.2 mm/s to find out the optimal speed for producing pure products.

3.2.2 The Effect of Gas Flow rate

In this study, arc discharge was done in de-ionized water with 1:1 ratio of a mixture of O_2 and N_2 gas supplied to the arc zone since this ratio provided pure

products along with the optimal speed which is previously investigated. For further investigation, the flow rate on properties of the as prepared ZnO nanoparticles is considered by varying in the range of 2-8 L/min.

3.2.3 The Effect of Arc Current in a Range of 20-60A

In this part, the effect of arc current supplied to the system on properties of the product is also investigated by varying in a range of 20-60 A.

3.2.4 The Effect of Water Temperature

The effect of surrounding water temperature where is the quenching zone of the products was varied from 2 ^{o}C, 15 ^{o}C and room temperature to investigate the properties and yield of the synthesized products.

3.2.5 The Effect of Oxygen Concentration

Owing to the optimal value the oxygen concentration for producing pure products which is 1:1 ratio of O2 and N2 gas (50 %wt O_2) was observed. An influence of oxygen concentration in the supplied gas was further varied from 50 to 100 %wt O_2 to investigate the effect on crystal structure of the synthesized ZnO nanoparticles.

3.3 Characterizations of Products

3.3.1 X-ray Diffraction Analysis (XRD)

The crystalline structure of the synthesized product is performed by X-ray diffraction (XRD, *Bruker* AXS *D8 Advance)* using CuK_{α} radiation of wavelength 1.5406 Å at 40 kV in the range of $2\Theta = 20° – 80°$. The crystallite size of the synthesized product was estimated from the full-width at half-maximum of the (101) diffraction peak according to the Scherrer equation.

$$D = \frac{k\lambda}{\beta \cos\theta} \tag{3.1}$$

Where k is a constant equal to 0.9, λ is the X-ray wavelength, β is the full width at half maximum and θ is the half diffraction angle.

3.3.2 Scanning Electron Microscopy (SEM)

The morphology of the product was investigated by scanning electron microscopy (SEM, Jeol JSM-6400) at Scientific and Technological Research Equipment Centre Foundation (STREC), Chulalongkorn University.

3.3.3 Transmission Electron Microscope (TEM)

The structure of the synthesized ZnO was investigated by Transmission Electron Microscope (TEM, JEOL: model JEM-2100) at National Nanotechnology Center (NANOTEC), (TEM, JEOL JEM-2100) at Scientific and Technological Research Equipment Centre Foundation (STREC), Chulalongkorn University, respectively.

3.3.4 Brumer-Emmett-Teller (BET) Analysis.

The specific surface area were determined by the N_2 absorption analysis with the Brunauer-Emmett-Teller model (BET, Belsorp mini II BEL Japan), pore size distributions were obtained from absorption/desorption branches of the isotherms using the Barret, Joyner, Halenda method (BJH).

3.3.5 Thermogravimetric Analysis (TGA)

The carbon content and thermal behavior of the obtained products were determined by using thermogravimetric analysis on a Mettler-Toledo TGA/DSC1 STARe System at Center of Excellence in Particle and Technology Engineering laboratory, Chulalongkorn University. The analysis was shown from temperature of 25 to 1000 ^{o}C under the gas flow of 40 ml/min of oxygen with 10 °C/min of heating rate.

3.3.6 Photoluminescence (PL)

The defect of ZnO was studied by photoluminescence measurement which was carried out on Spectrofluorometer (Jasco FP-6200) at Central Instrument Facility (CIF) faculty of science, Mahidol University. The Photoluminescence spectra were measured from 5mg ZnO dispersed in 10 ml ethanol at room temperatures in a spectral range of 350–600 nm excited by Xenon lamp source with a wavelength of 325 nm. The further operating conditions of measurement are shown as followings:

Excited band width: 5.0 nm
Emission band width: 5.0 nm
Scan speed: 125 nm/min

3.3.7 UV-Vis Spectrophotometer Analysis

The band gap of the synthesized photocatalysts were measurement by UV-VIS spectrophotometer analysis on UV-Vis-NIR (Cary 5000, Agilent Technologies, Australia), wavelength between 220 and 800 nm and step size of 1 nm at National Nanotechnology Center (NANOTEC). The spectra recorded at wave number 400-800 cm^{-1}.

3.4 Photocatalytic Activity Measurements

3.4.1 Photodegradation Apparatus

The schematic of equipment set up for the photocatalytic degradation used in this work is shown in Figure 3.2.

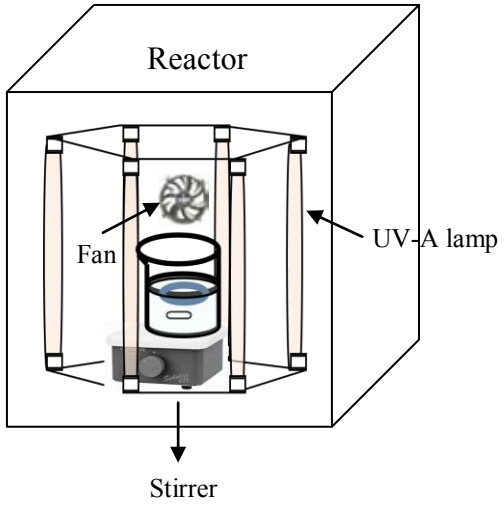

Figure 3.2 Schematic diagram of the photodegradation apparatus.

The reactor for photodegradation in this work is consists of 6 UV-A lamps (Phillips TLD 15W/05) used as a light source of the photocatalytic reaction. Fans are used to control temperature during the experiment. A magnetic stirrer used to generate turbulent conditions in mixture during the experiment to keep mixture homogeneous.

3.4.2 Photocatalytic Degradation Experiment

The photocatalytic activities of the as-prepared ZnO nanostructures are evaluated by degradation of methylene blue (MB) solution under UV irradiation. A mixture of 30 mg ZnO products used as catalyst and 200 ml of 10 ppm of MB solution ($C_{16}H_{18}N_3SCl.3H_2O$) was put in a 250 ml Pyrex beaker. The solution was magnetically stirred in the dark for 30 min to reach the adsorption equilibrium of MB on the catalyst. Then the solution was irradiated with six UV-A lamps (Phillips TLC 15w/05) and continuously stirred by a magnetic stirrer to keep the catalyst uniformly dispersed within the solution. After that, the degradation rate of methylene blue was measured by UV–Vis spectrophotometer (Shimadzu, UV-1700) at the maximum absorption wavelength of MB (664 nm).

CHAPTER IV

RESULTS AND DISCUSSION

Zinc oxide (ZnO) nanoparticles synthesized from arc discharge process was analyzed. The effects of synthesis conditions and parameters on characteristic of the as prepared products were investigated. In addition, the photocatalytic activity of the synthesized zinc oxide is also studied and discussed in this chapter.

4.1 Synthesis of ZnO nanoparticles by Arc Discharge in Water

For arc discharge in water, ZnO nanoparticles were produced from the formation of Zn vapor, which is generated from Zn rod at anode by very high temperature during the arc discharge, reacted with oxygen gas which is supplied to the system. The ZnO products synthesized via this process are formed at the arc zone and then conveyed to the surrounding water by the gas supplied, resulting in quenching of the ZnO nanoparticles. The products can be separated into two types; fine powders suspending in the deionized (DI) water and the settlings at the bottom. For this experiment, the deposit inside cathode hole is neglected since it was barely found.

4.1.1 Characteristics of the Synthesized ZnO Nanoparticles

The XRD patterns of ZnO nanoparticles synthesized under the condition of 1.2 mm/s of anode speed, 40A of arc current and 6 L/min of gas flow rate with 1:1 ratio of oxygen (O_2) and nitrogen (N_2) gas are shown in Figure 4.1. The diffraction peaks of the products that suspended in the water and settling at the bottom are represented in Figure 4.1a and 4.1b, respectively.

For suspended product in Figure 4.1a, it is clearly seen that there are only the diffraction peaks correspond to pure crystalline ZnO in wurtzite structure which is in agreement with the data from JCPDS card No. 36-1451. On the other hand, Figure 4.1b shows the diffraction peaks of crystalline zinc together with ZnO detected from the product settling at the bottom. Furthermore, the mixture of ZnO nanoparticles and solid Zn in settling position cannot be separated. Thus, the suspended product

which is consisted of ZnO in very high purity is the main product for characterizations.

From the experiment, it is suggested that zinc vapor is generated from zinc rod at anode by immense heat during the arc and react with O_2 gas to form ZnO nanoparticles. Nevertheless, zinc rod cannot completely generate zinc vapor, it is only melted and dropped down to the surrounding water during the arc discharge. Hence, the diffraction peaks of crystalline zinc are attributed to an incomplete reaction of the zinc vapor and the zinc solid dropped from the zinc rod. The average crystallite size of synthesized ZnO was calculated from the half-height width of the diffraction peak of XRD pattern by using the Debye-Scherrer equation which is proposed in Eq. 4.1.

$$D = \frac{k\lambda}{\beta \cos\theta} \tag{4.1}$$

Where k is a constant equal to 0.9, λ is the X-ray wavelength (1.5406A°), θ is the diffraction angle and β is the full width at half maximum. Based on (101) peak, the average crystallite size calculated by using the Scherrer equation was 35.22 nm.

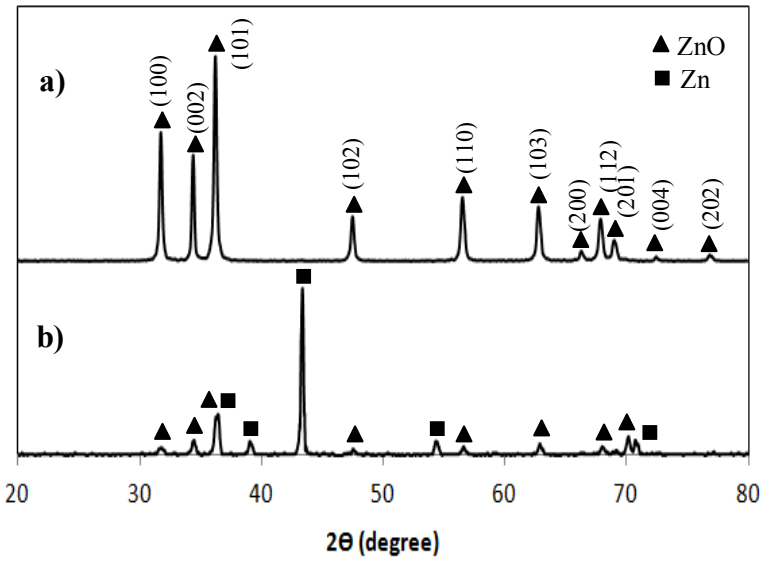

Figure 4.1 XRD patterns of the synthesized product (a) suspending in water and (b) settling at the bottom.

According to the XRD results, the morphology of the synthesized products was observed from the suspending position by scanning electron microscopy (SEM) and transmission electron microscope (TEM). SEM micrographs and EDX spectrum of the suspending product synthesized at 40A of arc current and 6 L/min of gas flow rate with 1:1 ratio of O_2 and N_2 gas are shown in Figure 4.2. As it can be seen from Figure 4.2a, the particles are mostly in the form of spherical shape and a small amount of ellipsoid. Furthermore, the size and morphology of the obtained ZnO particles are uniform. The measurement of the particle size from the SEM images could not be done due to agglomeration of the particles. The EDX (Energy-dispersive X-ray) spectrum of the synthesized ZnO obtained from arc discharge process in Figure 4.2b demonstrates that the sample compose of Zn and O while the presence of Au peak come from the sputtered coating for preparing the specimen for EDX analysis process. The weak signal at 0.25 keV confirms that there is trace carbon in the sample probably attributing to the graphitic carbon of cathode was corroded due to an immense heat about 3000-5000 K during arc discharge [42].

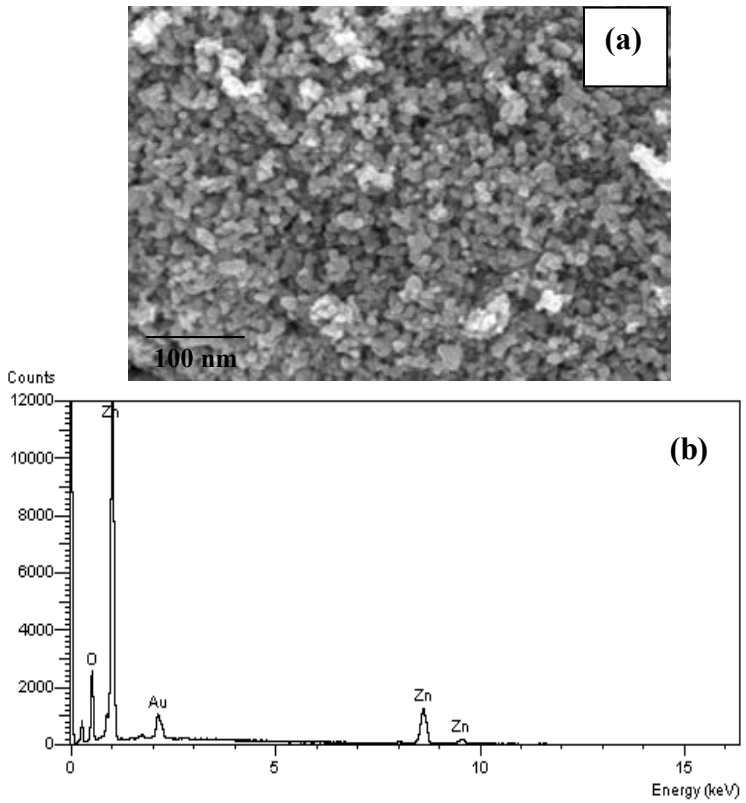

Figure 4.2 Typical SEM images of the synthesized ZnO, which suspending in the water (a) low magnification and (b) EDX spectrum.

TEM analysis of the suspended product synthesized at 40A of arc current and 6 L/min of gas flow rate with 1:1 ratio of O_2 and N_2 gas was also investigated. Figure 4.3(a-c) show TEM images of the sample in different magnification. It can be observed that the morphology of the ZnO particles is rod-like along with semispherical shape. Furthermore, Figure 4.3b indicates that the synthesized ZnO was cover with carbon layer which is in agreement with the presence of carbon peak from EDX analysis. This amorphous carbon was observed as the impurity in the products. In addition, the selected area electron diffraction (SAED) pattern indicates the poly-crystalline nature for ZnO as shown in Figure 4.3d.

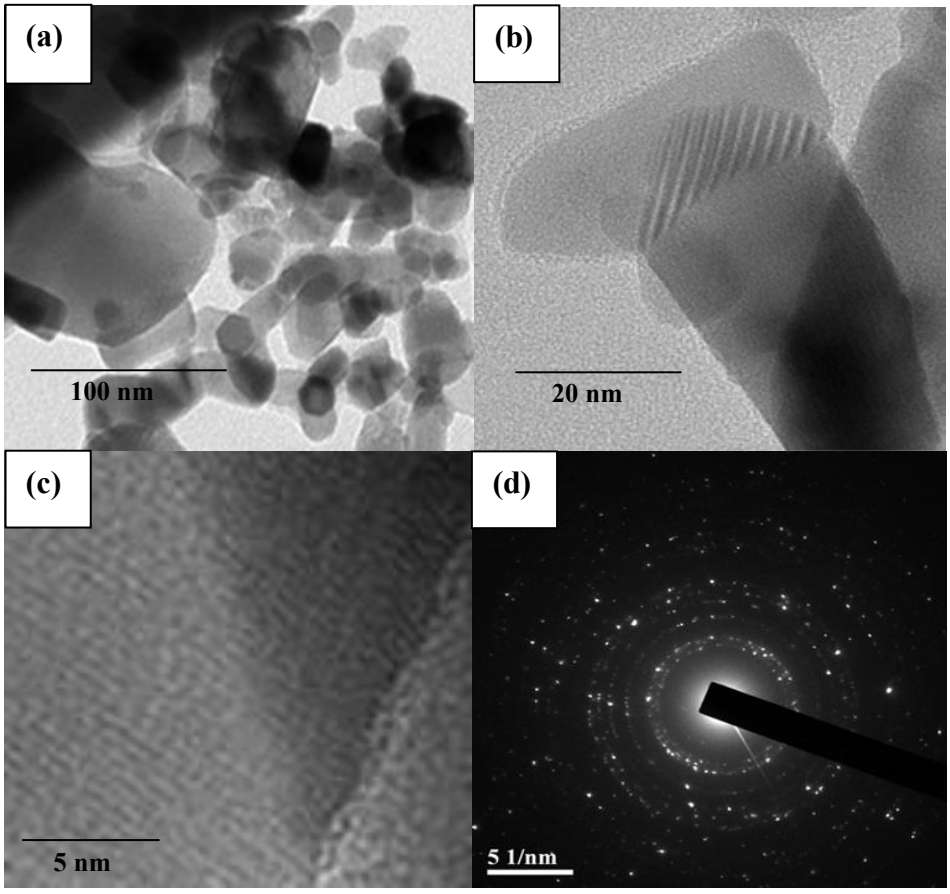

Figure 4.3 (a-c) TEM images with different magnification view and (d) SAED pattern of the as-prepared ZnO.

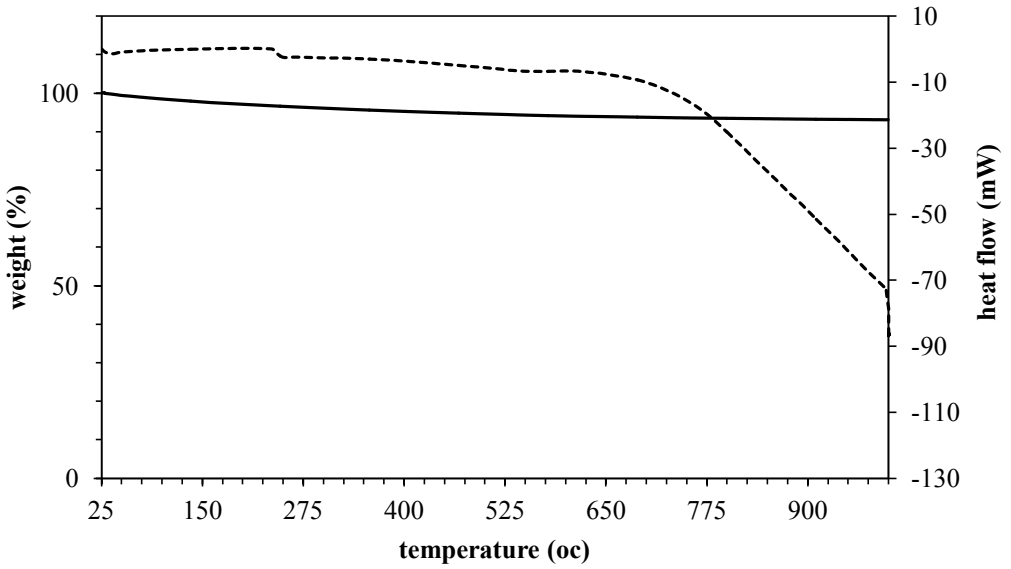

Figure 4.4 TGA curve of the synthesized ZnO nanoparticles after calcined at 500°C for 2 hours: (——) weight percentage and (·····) heat flow.

Accordingly, the TGA analysis is investigated to confirm the amount of carbon that adulterated in the ZnO products. The operation is done under 40 L/min of O_2 gas flow rate and heated from 25-1000 ^oC with 10°C/min of the heating rate. The result is shown in Figure 4.4 which can be observed that the curve is slightly decrease after operated until around 500 ^oC and remain stable to the last of the operation. This small weight loss about 7% of total weight could be attributed to an amorphous carbon in the sample.

As noted in Chapter III, calcination at 500°C for 2 hours in a box furnace with 10°C/min of the heating rate was used to eliminate moisture and carbon impurity from the obtained products. To assure that amorphous carbons can totally be removed from the products after calcination, the functional groups of products before and after calcination at 500 °C were investigated by FT-IR as shown in Figure 4.5.

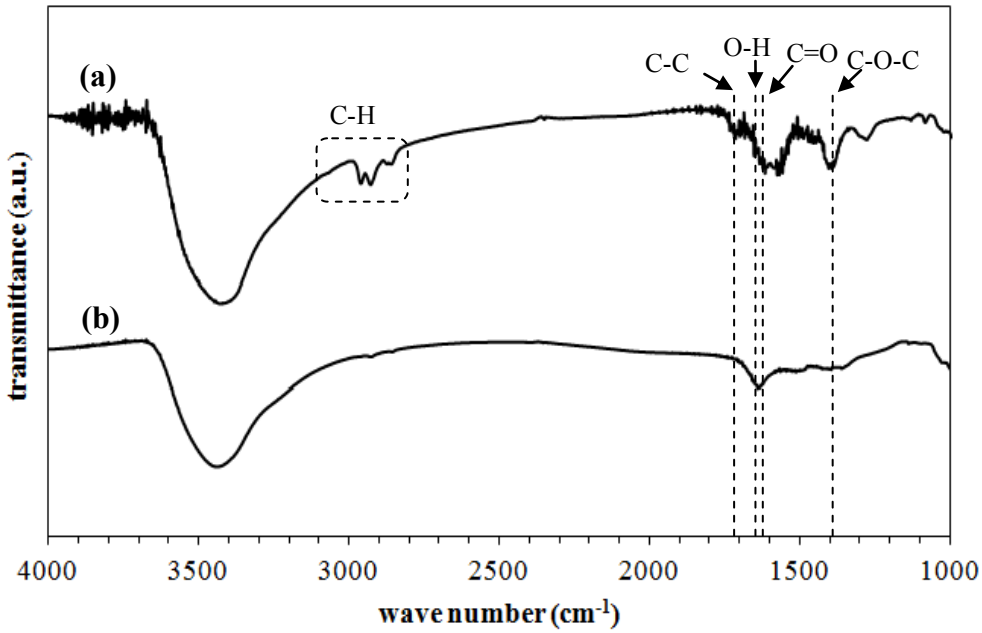

Figure 4.5 FT-IR spectra of the synthesized products (a) without calcinations process (b) after calcination at 500 ^{o}C.

According to Figure 4.5(a), both spectra exhibit a broad peak at 3400 cm^{-1} also appears due to O–H stretching mode. Considering at carbon functional groups, FT-IR spectra of ZnO corresponding to C–O–C, C=O and C-C stretching at wave number around 1385, 1626 and 1700 cm^{-1}, respectively. Besides, the vibration mode of the stretching-type C-H bond in the range of 2830-2970 cm^{-1} is also observed. On the other hand, the spectra of products after calcination in Figure 4.4b exhibits only peak at ~1633 cm^{-1} which is attributed to O–H bonding vibrations of adsorbed water molecules on ZnO particles or on KBr wafers [43]. It could be concluded that carbon is removed after calcination as noticed in the absence of C–O–C, C=O, C-C and C-H bond.

4.1.2 Effect of Anode Speed

The effect of anode speed was investigated to find the optimum value for providing pure ZnO nanoparticles of collection at suspended position. Figure 4.6(a-c) indicate the XRD patterns of the synthesized ZnO at different anode speed of 0.7 mm/s, 1.0 mm/s and 1.2 mm/s, respectively. The experiment was done under 40A of arc current and 6 L/min of gas flow rate with 1:1 ratio of O_2 and N_2 gas.

As can be seen in Figure 4.6, the ZnO peak together with Zn peak is detected when the anode speed at 0.7mm/s and 1.0 mm/s was used. However, there are only ZnO peaks when the experiment was operated at 1.2 mm/s of anode speed. The quantitative analysis from XRD of the products synthesized at different of anode speed are shown in Table 4.1. It is indicated that the formation rate of ZnO was increased in proportion to the increase of anode speed.

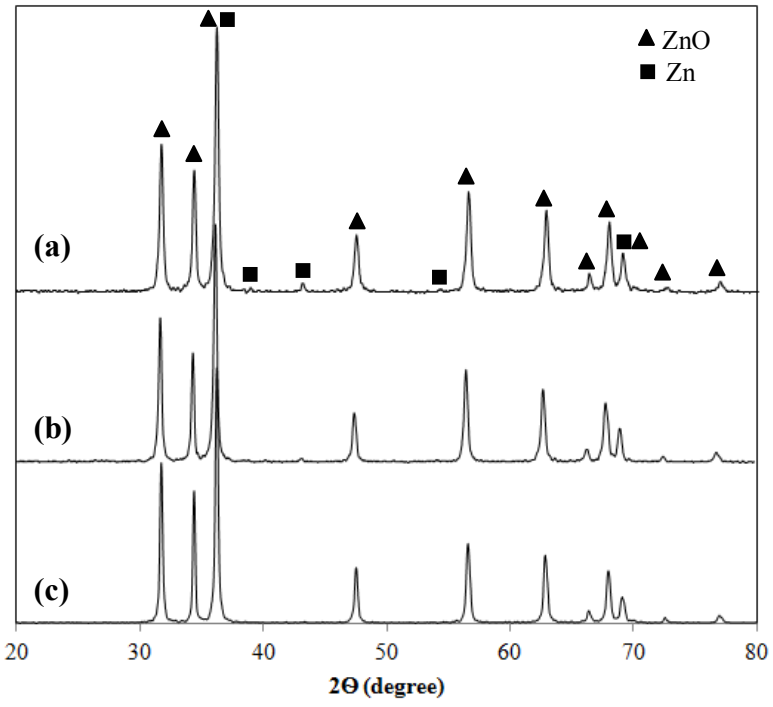

Figure 4.6 XRD patterns of the synthesized product at different anode speed (a) 0.7 mm/s, (b) 1.0 mm/s and (c) 1.2 mm/s.

Table 4.1 Quantitative analysis from XRD of ZnO and Zn products at different anode speed

Anode speed (mm/s)	Percentage of ZnO	Percentage of Zn
0.7	99.72	0.28
1.0	99.86	0.14
1.2	100.00	0.00

In the case of using higher anode speed during the operation, the reaction of Zn vapor which is generated from Zn rod at anode and oxygen in the gas supply tends to take place more continuously than that operated at relatively low speed. When the gap between cathode and anode is about 1-2mm, the arc was initiated then Zn rod was consumed and led to increase the gap between anode and cathode while anode was moving upward for keeping the proper spacing(1-2mm). In the case of using higher speed, it would take less time to reach the proper spacing. Hence, the reaction should rather be complete comparing to that of operated at low anode speed.

As the result, it was confirmed that the anode speed can affect the synthesis of ZnO nanoparticles. The continuous and complete reaction is influenced by this parameter. It can be concluded that the suitable value of anode speed for synthesis of pure ZnO nanoparticles by arc discharge process is confirmed to be 1.2 mm/s. For exceed anode speed, the Zn impurity was found when used with the varying of other parameters. Thus, 1.2 mm/s of anode speed were then chosen and set for all experiment along arc discharge process.

4.1.3 Effect of Arc Current

One of the important factors that affects the morphology as well as particle size of the synthesized ZnO nanoparticles is the supplied arc current from the direct current (DC) power supply. In this experiment, the influence of the arc current was studied under the condition of 1.2 mm/s of anode speed and 6 L/min of gas flow rate with 1:1 ratio of O_2 and N_2 gas. The arc current was varied in the range of 20A, 30A, 40A, 50A and 60A.

The morphology and particles size distribution of the ZnO nanoparticles prepared under different arc current were investigated by SEM and TEM analysis. Figure 4.7 (a-e) represent typical SEM images of ZnO nanoparticles synthesized at 20A, 30A, 40A, 50A and 60A, respectively. It can be seen that the particles are in spherical shape as well as small amount of ellipsoid. Nevertheless, the particle size cannot be measured from SEM image due to the agglomeration of the particles. The morphology of the ZnO particles was also investigated from TEM images as represented in Figure 4.8 (a-e). The corresponding histograms of size distribution of the particles are shown along with the TEM images. Resemble in SEM analysis, the particles were found to be ellipsoid shape along with spherical shape. The particles size distribution, measured from TEM images, show that the synthesized ZnO particles are about 20-50 nm in size. Besides, the average particle size of the ZnO product was increased with the increase in arc current.

When high arc current was used, they seem to promote more energy and hence greater amount of Zn vapor was generated. Consequently, highly concentrated Zn vapor gathers together and reacts with supplied oxygen to form larger ZnO particles. Moreover, the number of semispherical nanoparticles is higher than ellipsoid nanostructures in higher arc currents. Generally, ZnO inclines to form rod-like structures due to its lattice geometry [10]. Nevertheless, spherical shape together with ellipsoid shape particles were found in this experiment due to the products was rapidly quenched in deionized water. This led to freeze their shape and reduced the growth rate of the particles. Thus, the products do not have enough time to form rod shape structures before stabilization.

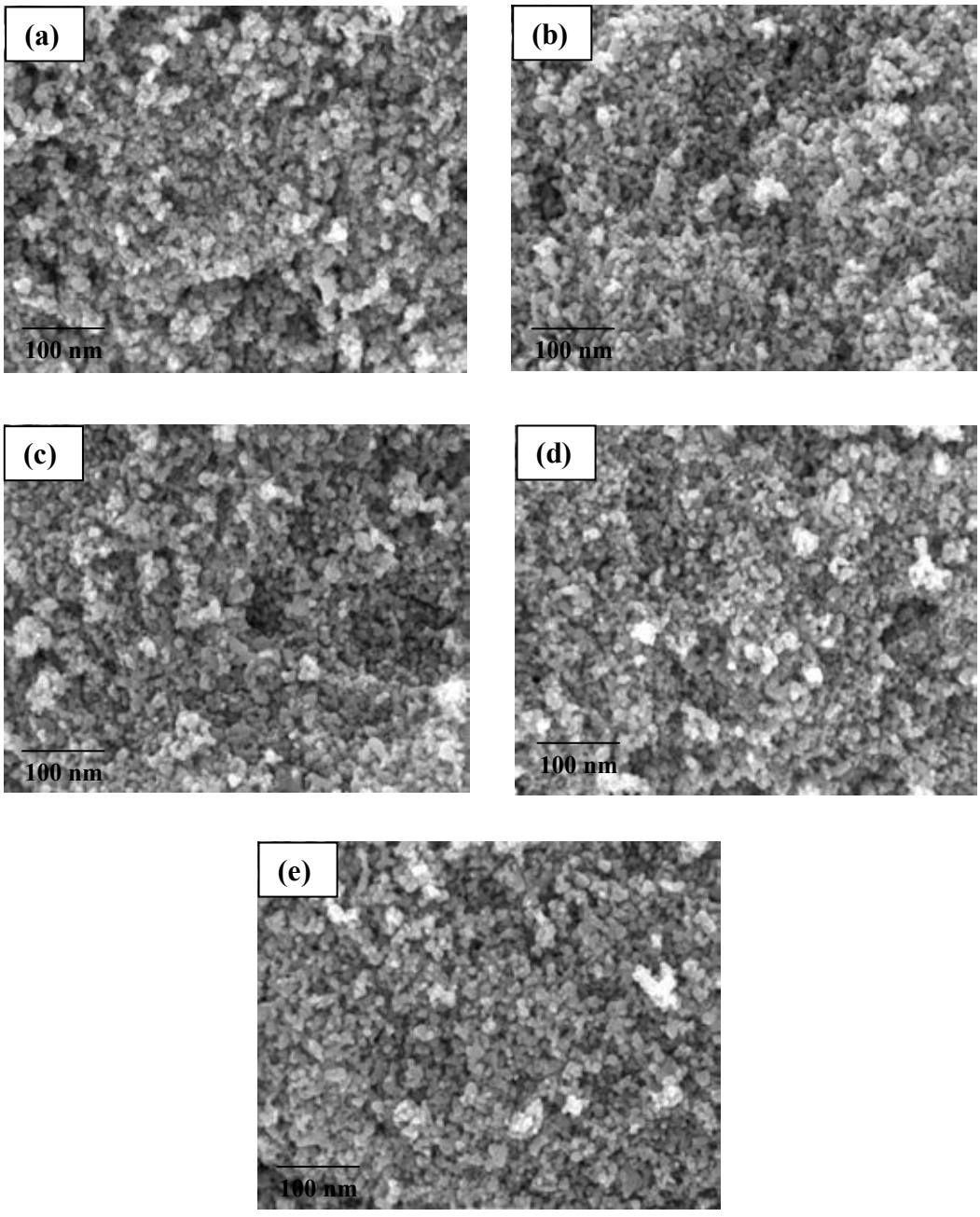

Figure 4.7 Typical SEM images of ZnO particles synthesized at 1.2mm/s of anode speed and 6 L/min of gas flow rate by using different arc current: (a) 20A, (b) 30A, (c) 40A, (d) 50A and (e) 60A.

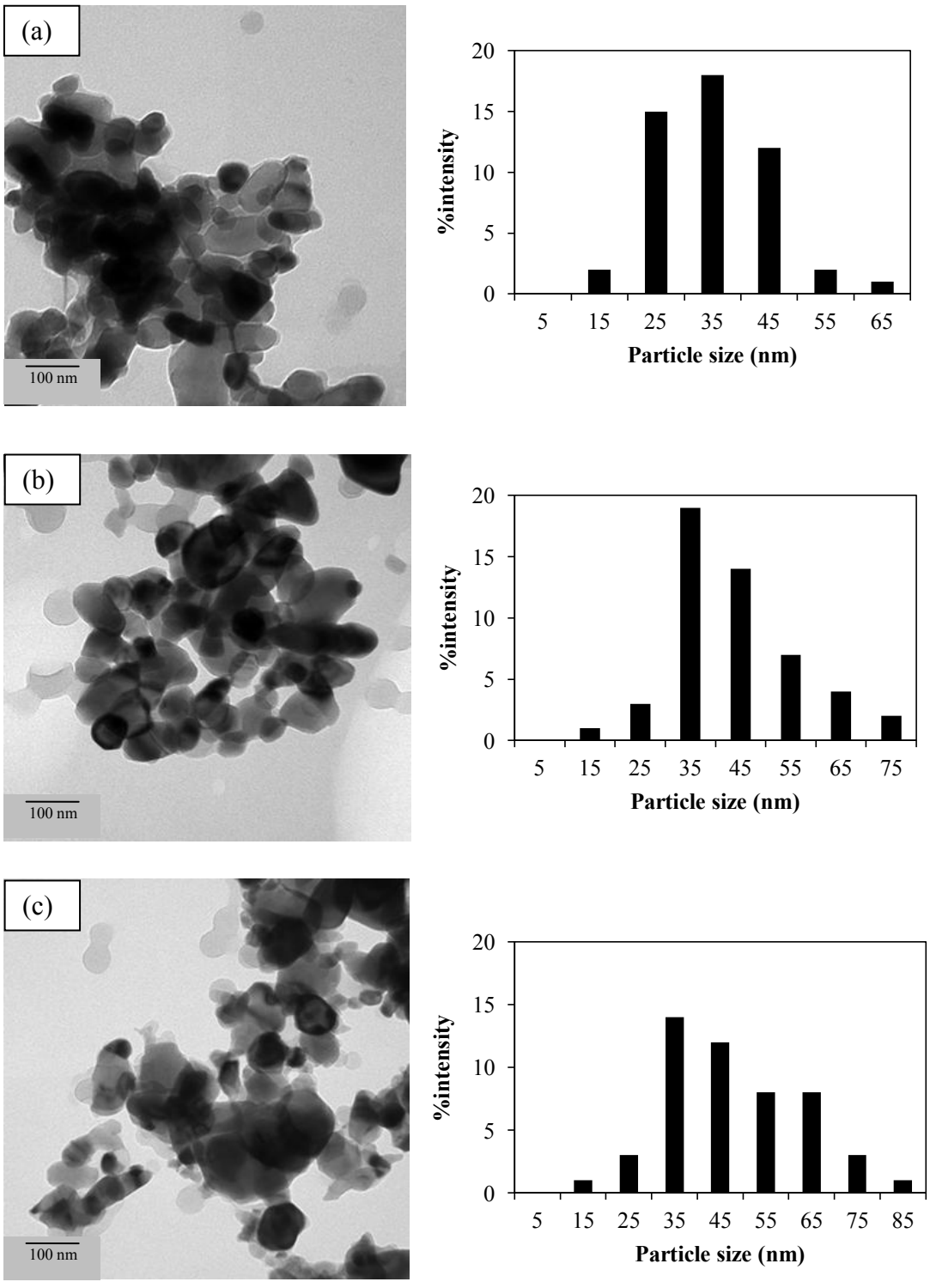

Figure 4.8 TEM images and particle size distribution of ZnO particles synthesized at 1.2mm/s of anode speed and 6 L/min of gas flow rate by using different arc current: (a) 20A, (b) 30A (c), 40A, (d) 50A and (e) 60A.

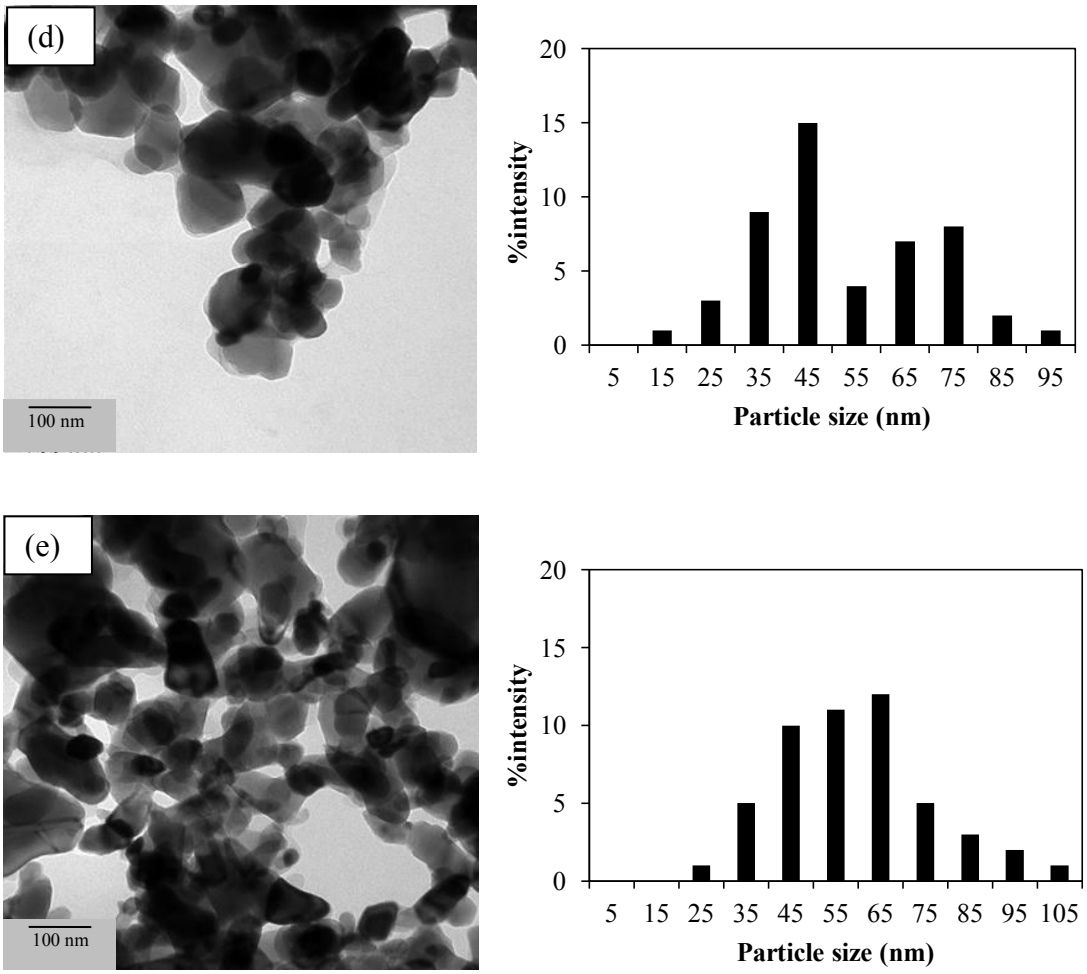

Figure 4.8 (Continued) TEM images and particle size distribution of ZnO particles synthesized at 1.2mm/s of anode speed and 6 L/min of gas flow rate by using different arc current: (a) 20A, (b) 30A (c), 40A, (d) 50A and (e) 60A.

Additionally, the use of high arc current could lead to provide discontinuity of the reaction. This could be described by the relationship between weight of zinc solid collected at the bottom and arc current as shown in Figure 4.9. The result shows that %weight of zinc solid is increase with higher arc current. The large amount of zinc solid was found at settling position became high arc current can generate more zinc vapor and also zinc liquid which is finally dropped down to the surrounding water by rapid quenching. When melted zinc was dropped, the gap between anode and cathode became larger and then the reaction was intermitted while anode was moving

upward to cathode. After that, the reaction would be started again when the gap was narrow enough (1-2 mm). Meanwhile, using of low arc current promote more continuous reaction hence less amount of Zn solid was found.

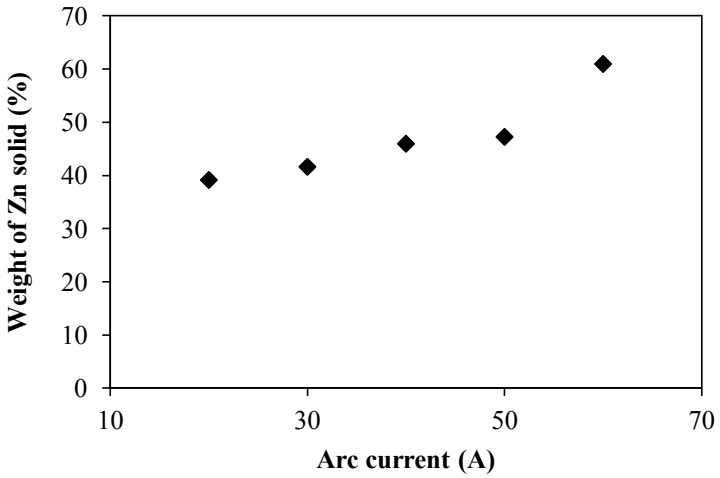

Figure 4.9 Relationship between weight of zinc solid and arc current supply.

An influence of arc current on the yield of the synthesized products was also observed from this experiment. The yield of ZnO nanoparticles will be determined from suspended products since we have found that it contained pure ZnO. The yield of ZnO nanoparticles is calculated from Eq.4.2.

$$\%Yield\ of\ ZnO = \frac{Wt.of\ suspended\ product - Wt.of\ carbon}{Consumed\ wt.of\ zinc\ anode - Wt.of\ zinc\ solid\ at\ bottom} \times 100 \quad (4.2)$$

The yield of the synthesized products with various arc currents is shown in Figure 4.10. As it can be seen, yield of ZnO nanoparticles is significantly increased reaching the highest values at 30A of arc current and then decreased with higher arc current. The decrease in yield of ZnO nanoparticles can cause by the discontinuous reaction from using high arc current as mentioned above. On the other hand, small value of the yield at 20A of arc current could be ascribed to the lower amount of zinc vapor generated comparing to that operated at 30A. Consequently, arc current at 30A is considered to be the optimum value for producing of ZnO nanoparticles in the process.

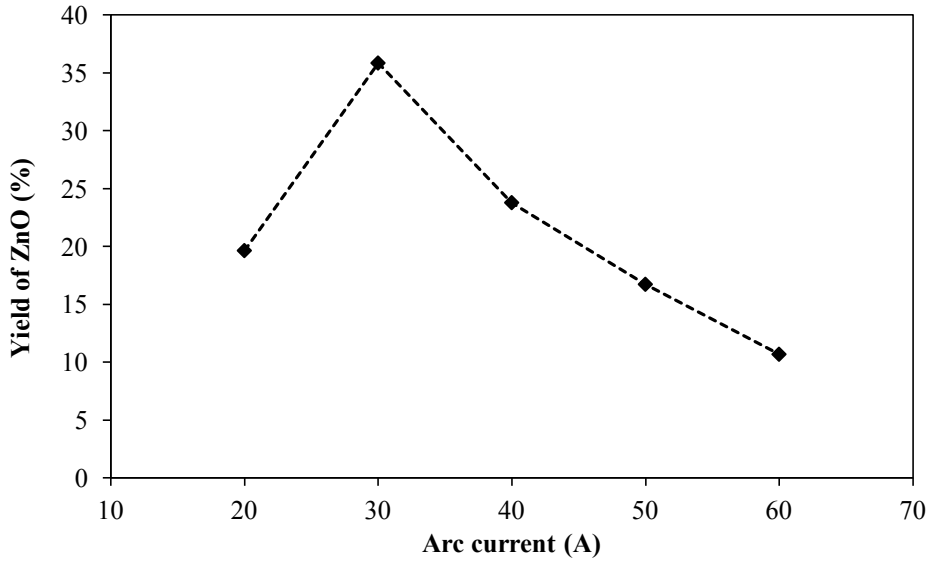

Figure 4.10 Influence of arc current on the yield of synthesized ZnO nanoparticles.

4.1.4 Effect of Gas Flow Rate

Another factor which can also affect the morphology and particle size of the as-prepared ZnO is flow rate of gas supplied to the system. In this experiment, arc discharge is operated under the condition of 1.2 mm/s of anode speed and 40A of arc current. The gas flow rate with 1:1 ratio of O_2 and N_2 gas was varied from 2 to 8 L/min. Figure 4.11 (a),(b),(c) and (d) show SEM images of the ZnO products which is prepared with gas flow rate of 2 L/min, 4 L/min, 6 L/min and 8 L/min, respectively. Morover, TEM images of ZnO products syhtesized with vary values of flow rate are represented in Figure 4.12.

Considering the effects of gas flow rate on morphology of the as-prepared products, the particle size of produced ZnO nanoparticles decreases from 84.36 to 39.74 nm when the gas flow rate is increased. Additionally, it was noticed that the quantities of semispherical nanoparticles are higher than ellipsoid shape. This can be explained by mean of quenching rate of the as-prepared product from the varying of gas flow rate. When carrier gas flow rate is high, it would provide higher velocity to convey the particle to the surrounding water. As a result, the formation of ZnO occurred in a very short and insufficient time to form larger particles as well as reduce the growth rate for the formation of ellipsoid shape.

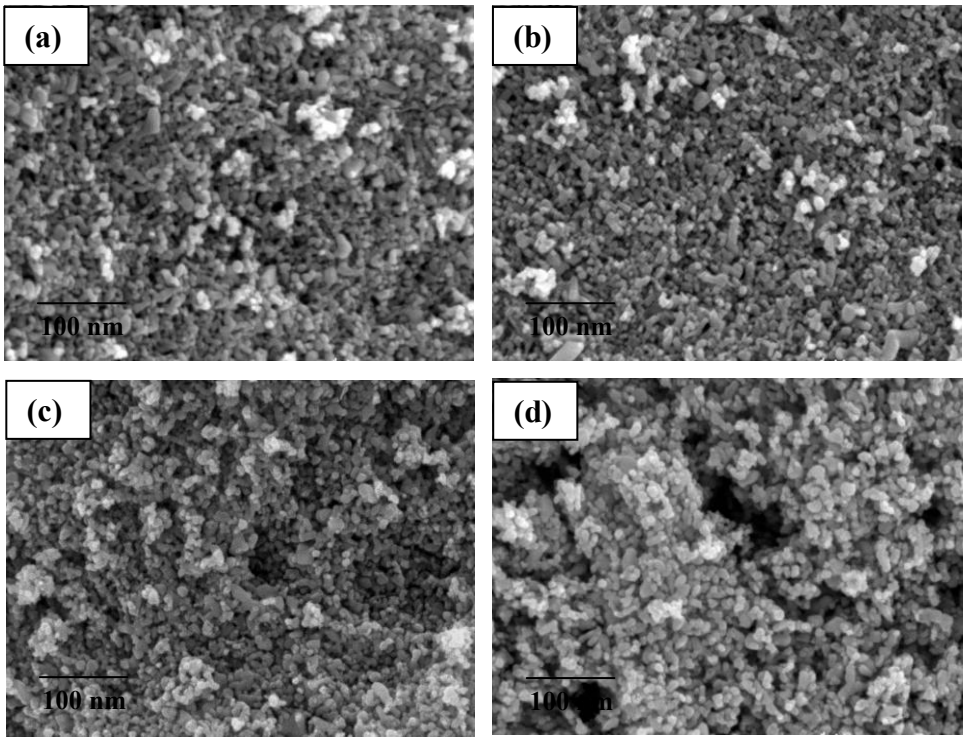

Figure 4.11 Typical SEM images of ZnO particles synthesized with flow rate of: (a) 6L/min, (b) 4L/min (c), 6L/min and (d) 8L/min.

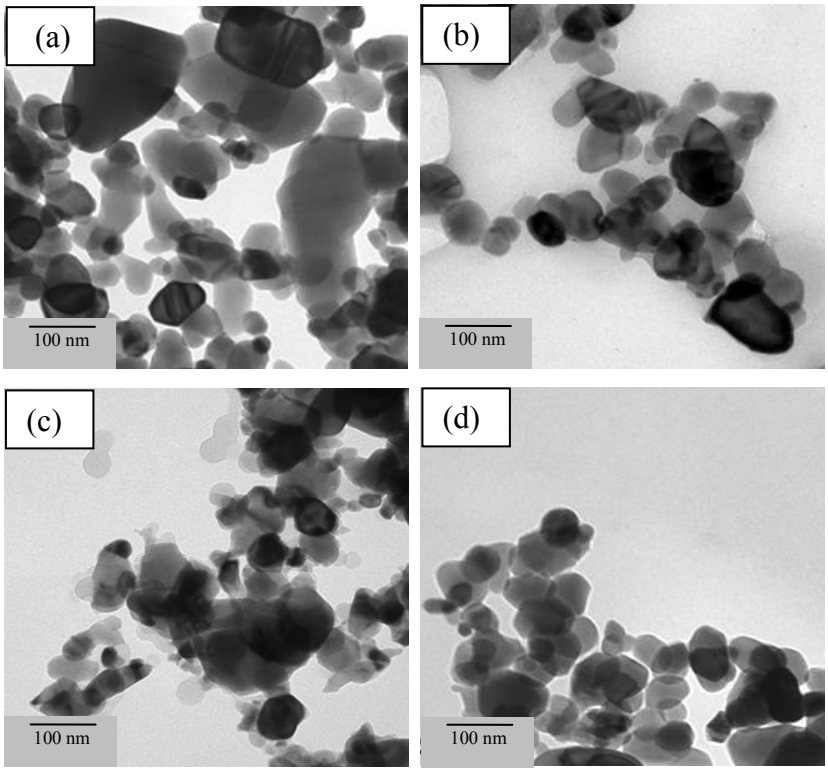

Figure 4.12 TEM images and particle size distribution of synthesized ZnO by varying gas flow rate: (a) 2L/min, (b) 4L/min (c), 6L/min and (d) 8L/min.

In order to further study the influence of gas flow rate on the synthesis of ZnO in more details. The yield of ZnO products was investigated and represented in Figure 4.13. The result shows that the yield of ZnO products is increased with an increasing of gas flow rate from 2 L/min to 6 L/min and decrease under condition of 8 L/min of gas flow rate. When the gas flow rate was low, the carrier gas do not have high velocity to convey ZnO from arc zone to quenching zone in deionized water causing small amount of ZnO product. As a result, more ZnO products are obtained from the synthesis under higher gas flow rate and the optimum values is 6 L/min. Nevertheless, After it exceed the optimum value, It would reduce the retention time for the formation of ZnO during the arc discharge and also expell ZnO products along with air, resulting in the decrease of percent yield of the synthesized products .

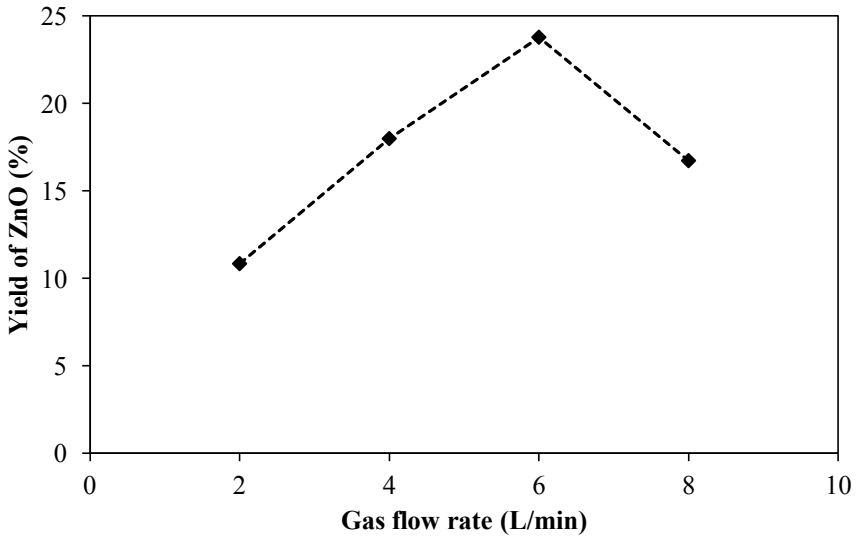

Figure 4.13 Influence of flow rate on the yield of synthesized ZnO nanoparticles.

4.1.5 Effect of Water Temperature

In order to study more about the effect of synthesis parameters on ZnO products, the effect of water temperature was investigated. In this experiment, the temperature of the liquid medium was varied in the range of 2 ^{o}C to 27 ^{o}C. The arc discharge was done under the condition of 1.2mm/s of anode speed, 40 A of arc current and 6 L/min of gas flow rate. The representative of SEM and TEM images of ZnO prepared under different water temperature are shown in Figure 4.14 and 4.15, respectively. It can be noticed that the particles are in spherical shape together with rod-like shape and no significant difference of the comparison between 2^{o}C, 15 ^{o}C and 27^{o}C was observed. The relationship between water temperature and particle size is shown in Figure 4.16. The average particles size measured from TEM images is 48.22 nm.

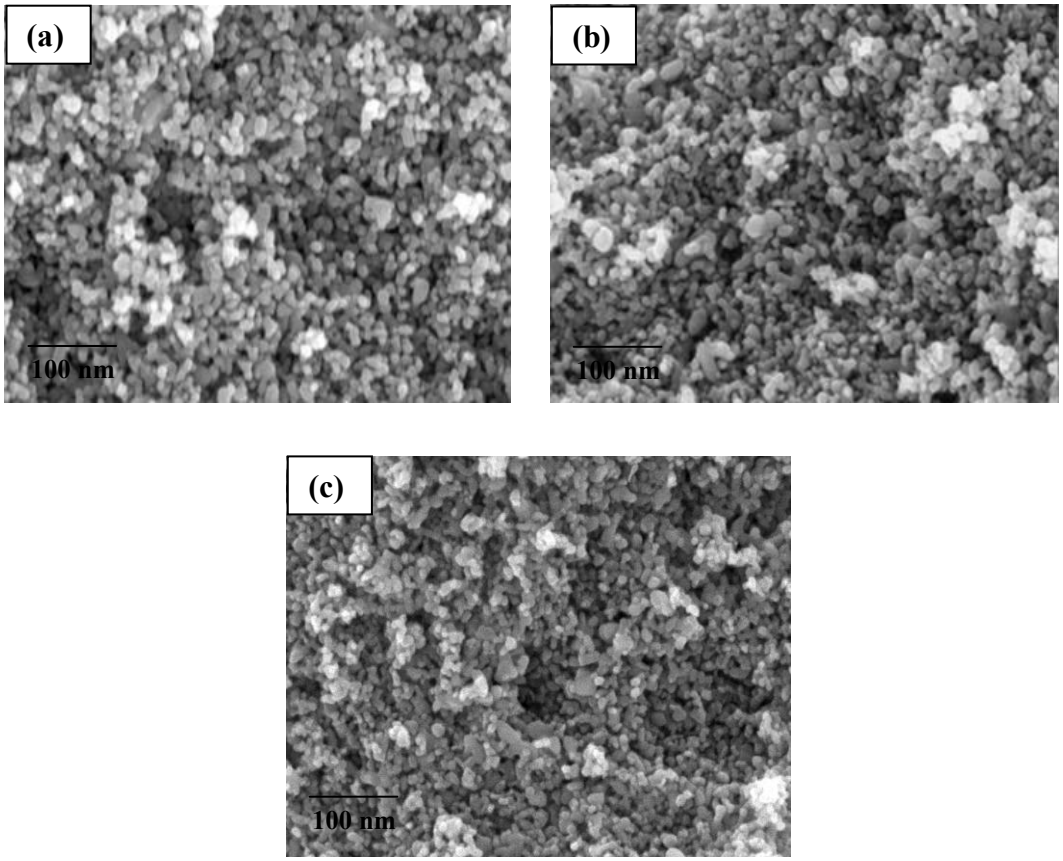

Figure 4.14 Typical SEM images of ZnO particles synthesized under different water temperature: (a) 2 ^{o}C, (b) 15 ^{o}C and (c) 27 ^{o}C.

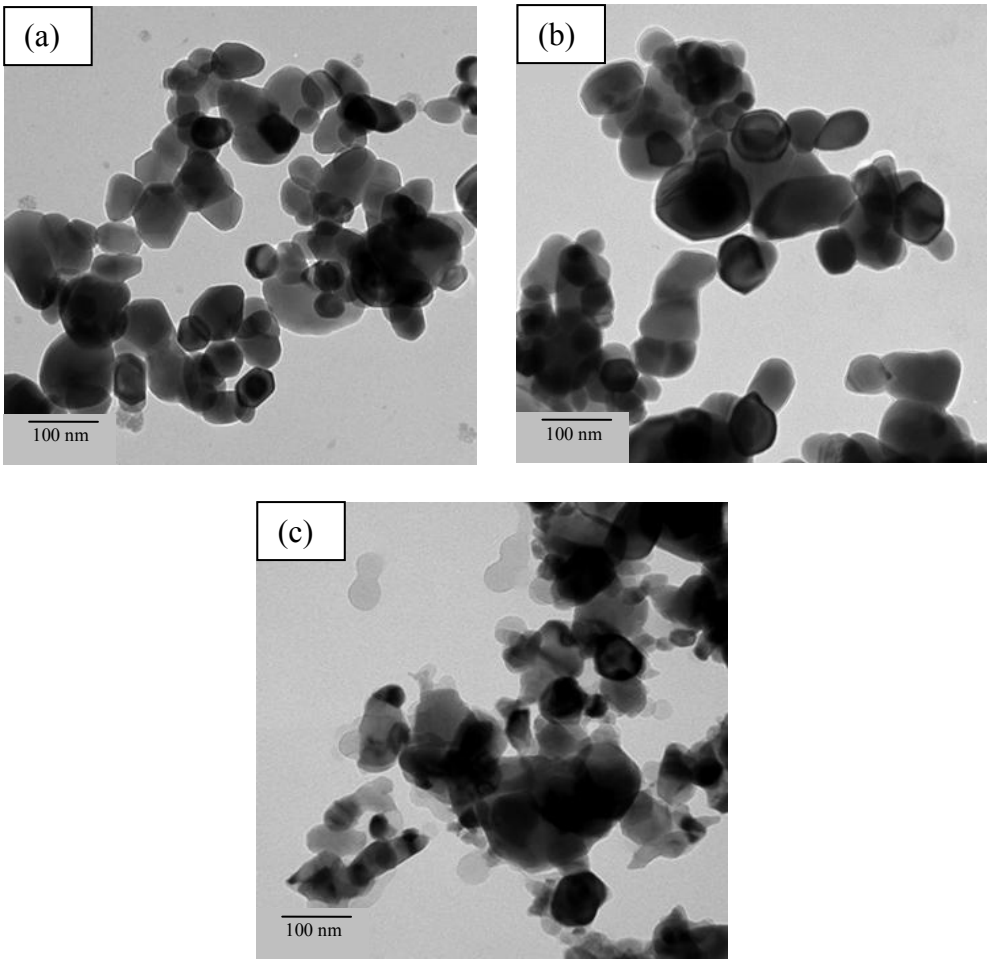

Figure 4.15 Representative for: TEM images of the synthesized ZnO at different water temperature (a) 2 ^{o}C, (b) 15 ^{o}C and (c) 27 ^{o}C

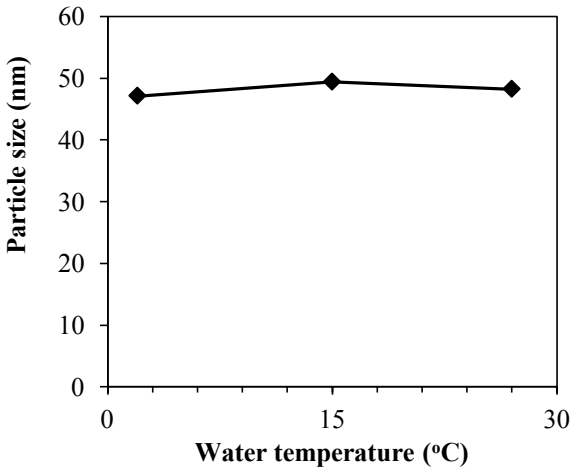

Figure 4.16 Relationship between particles size of ZnO and water temperature.

In addition, the yield of ZnO nanoparticles produced by using different temperature of DI water in arc discharge process is studied and depicted in Figure 4.17. The yield of ZnO products is gradually increased with an increasing of water temperature. It has been report that O_2 was not produced by the electrolysis of water from arc discharge in water process [34]. Hence, the formation of ZnO nanoparticles of this experiment was mainly from the reaction between Zn vapor and O_2 in the gas supply.

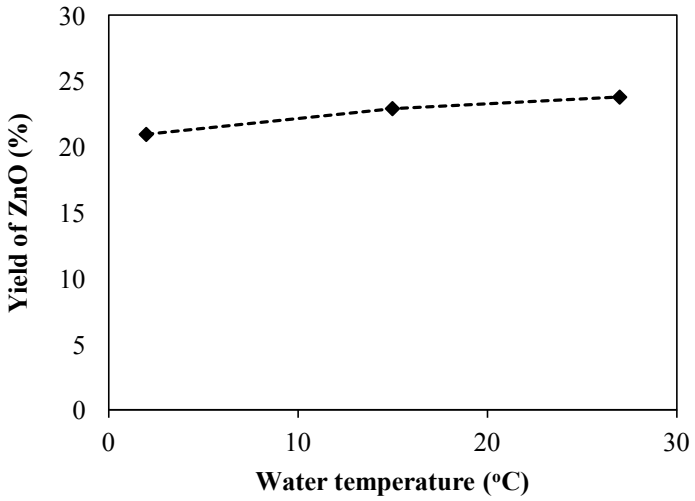

Figure 4.17 Influence of water temperature on the yield of synthesized ZnO nanoparticles.

Furthermore, water vapor can also be generated during the operation of arc discharge and it relatively increase to water temperature [34]. This can be explained that water vapor could diffuse from downstream zone where it is generate into the reaction zone and reacted with Zn vapor to form ZnO nanoparticles as shown in Figure 4.18. In consequence, large amount of water vapor in high water temperature condition could lead to promote formation of ZnO nanoparticles. The mechanism of reaction is presented in Eq. 4.3.

$$Zn(g) + H_2O(g) \rightarrow ZnO(s) + H_2(\mathrm{g}) \tag{4.3}$$

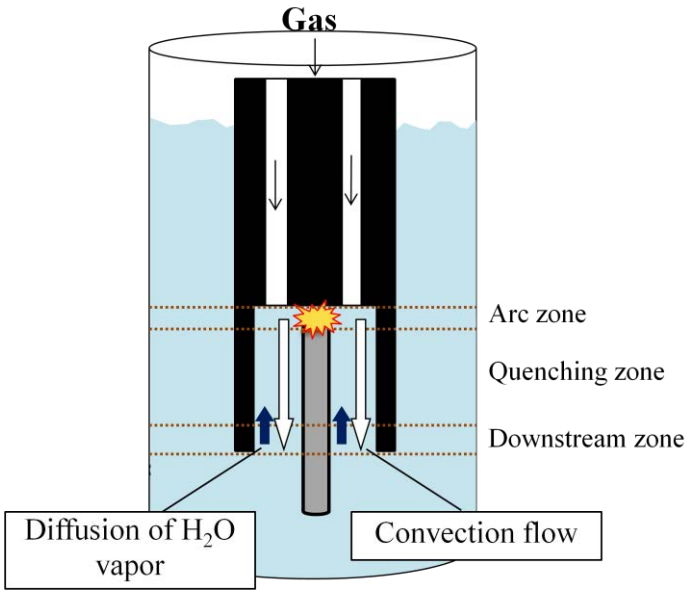

Figure 4.18 Schematic of the reaction field in arc discharge in water with three categorized zones.

4.1.6 Effect of Oxygen Concentration

In this part, variety of oxygen concentrations in gas flow rate were used for further investigates the influence of the synthesis parameter on ZnO products in more details. The effect of oxygen concentration which could affect crystal structure of ZnO product is studied. After an observation for synthesis of pure ZnO nanoparticles, we have found that at 50% O_2 in the gas mixture of O_2 and N_2 is the minimum value to generate pure ZnO of this experiment. Thus, the oxygen concentration will be varied from this minimum value to 100% of O_2 under the condition of 40A arc current with constant flow rate at 6 L/min. Figure 4.19 demonstrates the comparison of photoluminescence (PL) spectra obtained from the produced particles at various oxygen concentrations under excitation wavelength of 325 nm. The spectra of the synthesized nanoparticles exhibit broad emission band in the range of 370-600 nm. The two significant peaks at c.a. 390 nm in UV range and c.a. 467 nm in visible range are observed.

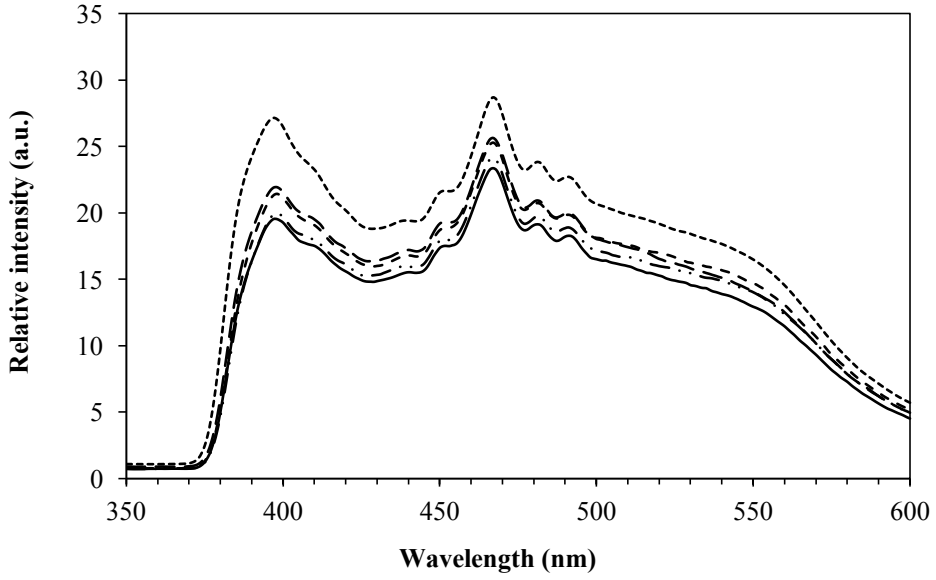

Figure 4.19 Photoluminescence spectra of the synthesized ZnO by varying oxygen content of gas supply: (——) 50%, (— · ·) 58.33%, (- - -) 66.67%, (— —) 75% and (.....) 100%.

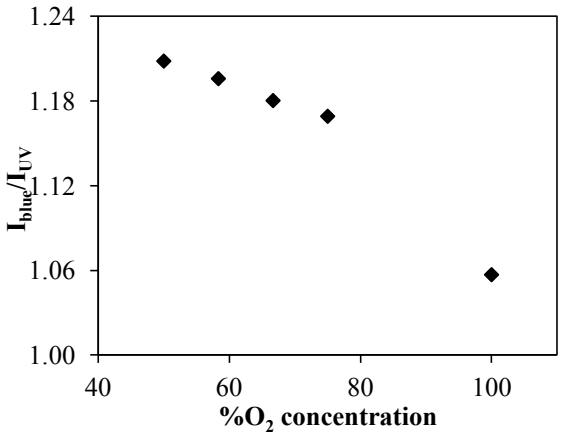

Figure 4.20 Relationship of I_{blue}/I_{UV} and O2 concentration used to synthesis of ZnO nanoparticles.

According to Figure 4.19, the PL spectra at 467 nm is noted to be the blue emission which is corresponded to the electron transition from the level of interstitial Zn (Zn_i) defect to the valence band of ZnO[20]. The formation of Zn_i defects occured due to the diffusion of Zn-rich atoms to ZnO lattice when the arc was initiated at high temperature. Moreover, the ratio of intensities of blue luminescence to that of UV luminescence (I_{blue}/I_{UV}) is presented in Figure 4.20. It can be clearly seen that I_{blue}/I_{UV} decreases with the increase of oxygen concentration from 50% to 100%. The fact that the smallest ratio of I_{blue}/I_{UV} come from the product prepared by using 100% O_2 suggestes that it provided sufficient oxygen to react with Zn atom and form ZnO nanoparticles before quenching in liquid medium.

Additionally, it has been reported that the surface defect can affect band gap energy (E_g) of the semiconductor since ZnO is the wide band gap semiconductors (3.34 ev) , the defect could be one of the most promising effect that can lead to modified band gap energy. The optical band gap of ZnO nanoparticles obtained from this experiment can be observed by using the Tauc's equation which illustrates a relationship between absorption coefficient and the incident photon energy as shown in Figure 4.19. The diffraction reflectance spectra in Figure 4.21(a-e) represent for products synthesized by using 50%O_2, 58.33%O_2, 66.67%O_2, 75%O_2 and 100%O_2, respectively. The intersection between the linear fit and the photon energy axis gives

the value to E_g about 3.23 eV. This value is smaller than that of the regular ZnO nanoparticles because of the interstitial Zn defect found in ZnO lattice.

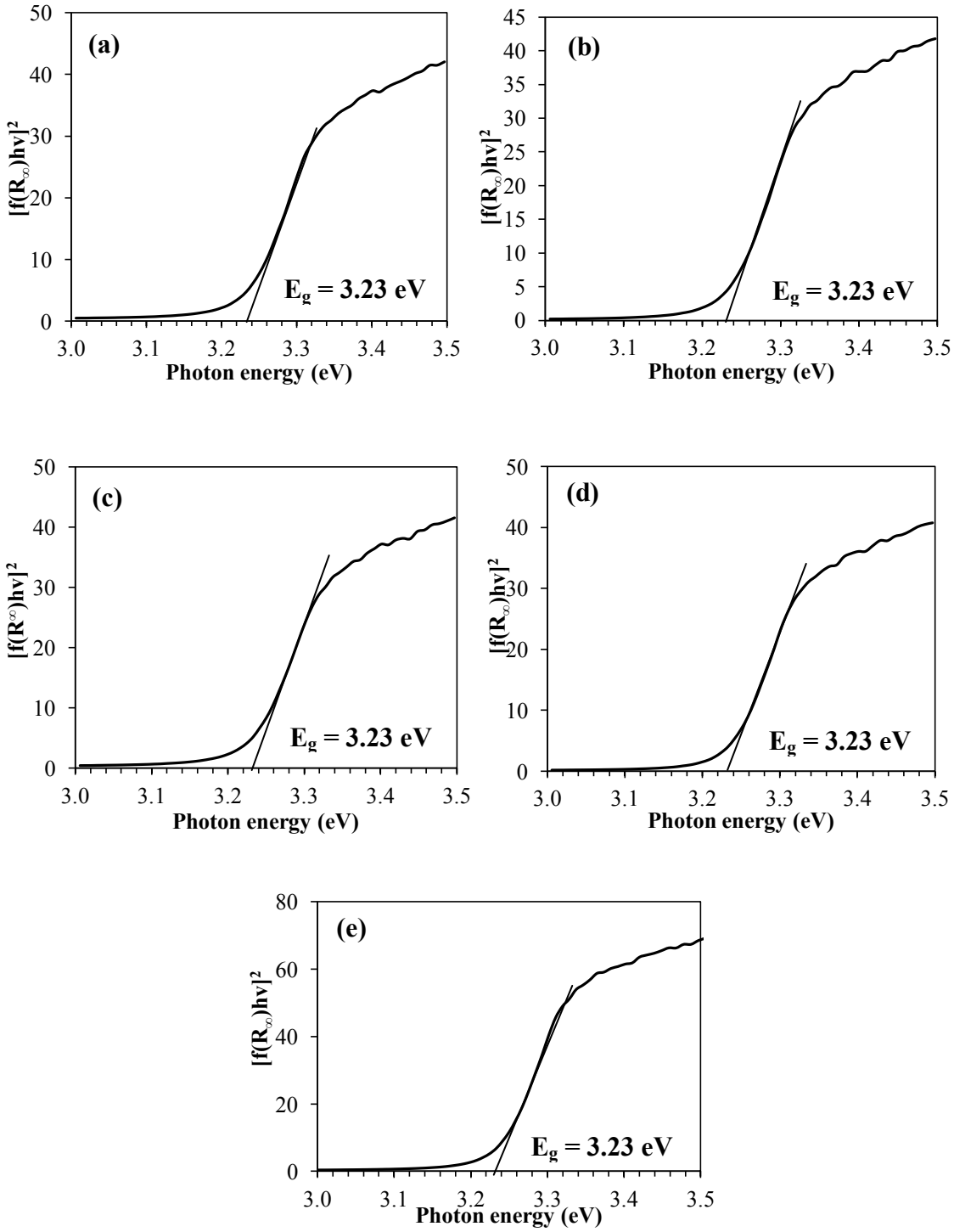

Figure 4.21 The relationship between hν and $(hvF(R_\infty))^2$ curve of synthesized ZnO (a) 50%O_2, (b) 58.33%O_2, (c) 66.67%O_2, (d) 75%O_2 and (e) 100%O_2.

4.2 Photocatalytic Activity of the as-prepared ZnO

Base on the theory of photocatalytic process, the photocatalysis efficiency depends on competition between the separation process and the recombination process of electron (e^-) and hole (h^+) after being induced by light at the surface of photocatalyst semiconductor. Consequently, desired photocatalysts are expected to promote the charge transfer processes while suppressing recombination process. To study the photocatalytic activity of the catalyst, it can be explained from kinetic of the photodegradation of organic pollutants which can simply be described by the pseudo-first order kinetic.

$$r = -\frac{dC}{dt} = k_{app}C \tag{4.5}$$

Where r is the degradation rate of the organic pollutants, C is the concentration of the organic pollutants being degraded, k_{app} is the apparent rate constant of this model, t is the UV irradiation time. For batch operation, Eq. 4.5 can be integrated to Eq. 4.6 when C_0 is initial concentration of organic compound.

$$\ln\frac{C_0}{C} = k_{app}t \tag{4.6}$$

Kinetics studies will be evaluated from the change in the concentration of the organic compound as a function of irridiation time. The apparent rate constant (k_{app}) can be determined from the slope of the plotted curve.

In this part, the photocatalytic activity of the as-prepared ZnO is investigated in order to study the effect of synthesis parameters on the degradation of methylene blue as a dye pollutant under UV light. The pseudo first order kinetic model is chosen to estimate photocatalytic activity of ZnO product due to the solution is highly diluted (10 ppm as mention in section 3.3.2) so adsorption term can be neglected. Effect of different parameters on the photocatalysis efficiency of the ZnO products which are calcination, particles size and Zn interstitial defect were ascertained.

4.2.1 Effect of Calcination Process

Depending on the preparation of ZnO from arc discharge process, it can be seen that the synthesized particles contained amorphous carbon as an impurity which can be eliminated by calcination as described in Section 4.1. To further investigate the effect of calcination on the property of ZnO product in more detail, the particles size, specific surface area and average pore diameter including the nitrogen adsorption-desorption isotherms of the synthesized ZnO were observed. Figure 4.22 shows the nitrogen adsorption-desorption isotherms of synthesized ZnO nanoparticles before and after calcination. The isotherm can be classified as type-II which is corresponding to non-porous material. Moreover, the specific surface areas of the synthesized ZnO before and after calcination at 500 ^{o}C evaluated from the Brunauer, Emmett and Teller (BET) method are shown in Table 4.2.

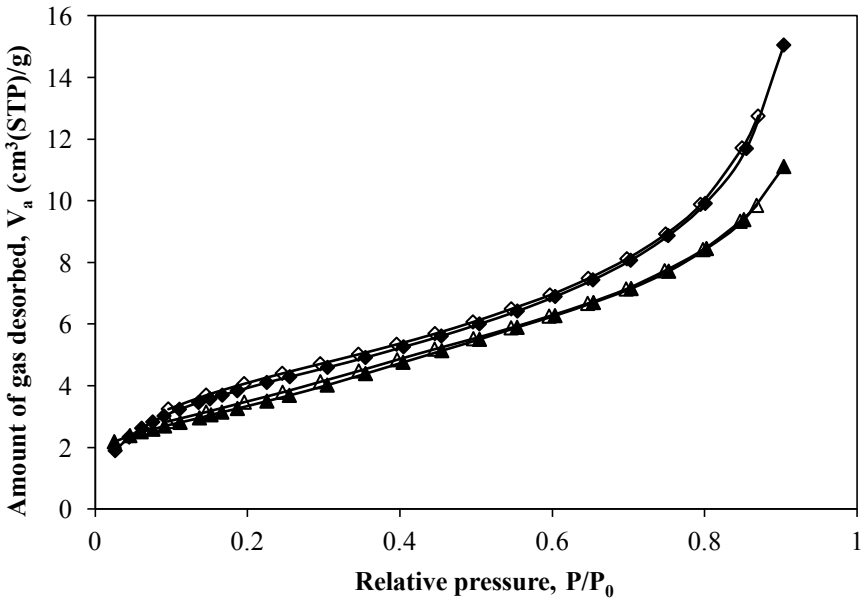

Figure 4.22 Adsorption/desorption isotherm of synthesized ZnO (–■–) before calcination and (–▲–) after calcination at 500 ^{o}C.

Table 4.2 Particles size and specific surface area of ZnO before and after calcination.

Type of ZnO	Particles size, (nm)	Specific surface area, S_{BET}, (m^2/g)	Average pore diameter (nm)
Before calcination	27.14	14.04	6.63
After calcination	48.21	10.54	5.66

In order to investigate the photocatalytic activity of ZnO products, the photodegradation of methylene blue in an aqueous solution was operated under UV-A irradiation and the concentration of methylene blue was measured the absorption spectra at certain interval using UV-Vis spectrophotometer. The initial concentration of methylene blue was fixed at 10 ppm. The mixture was kept in the dark for 30 min to allow complete adsorption of methylene blue on the surface of the photocatalysts. Figure 4.23 exhibits the photodegradation of methylene blue by using ZnO products before and after calcination.

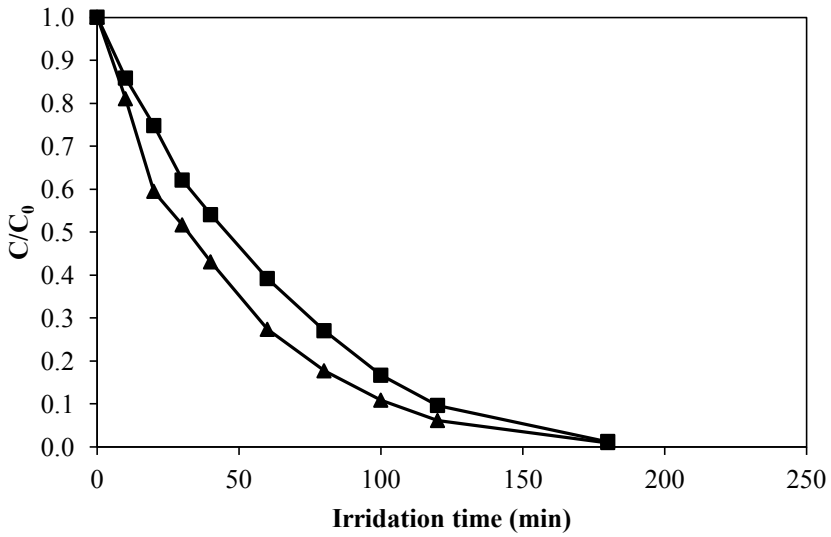

Figure 4.23 Process of photocatalytic degradation of methylene blue under UV light illumination over different photocatalysts: (–■–) ZnO before calcination and (–▲–) ZnO after calcination.

The results show that methylene blue in aqueous solution can be completely eliminated by both catalysts after illumination by UV-A light within 180 min. However, the apparent rate constant (k_{app}) determined from the slopes of the degradation data for synthesized ZnO which is calcined at 500 ^{o}C ($k_{app(MB)}$ = 0.0239) is higher than that of ZnO before calcination ($k_{app(MB)}$ = 0.0209) as shown in Figure 4.24. It is indicated that the reaction using ZnO which is calcined at 500 ^{o}C as catalyst is faster than that using ZnO without calcination. Hence, the synthesized ZnO after calcination has higher activity in degrading methylene blue with the correlation coefficient from pseudo first-order model presented in Table 4.3.

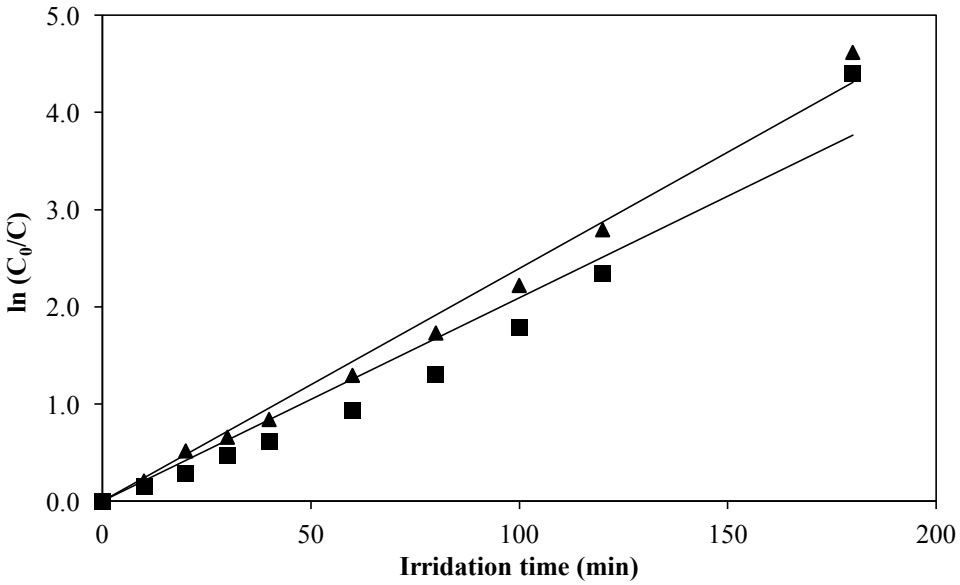

Figure 4.24 First-order linear transforms plot of the photocatalytic degradation on the Synthesized ZnO: **(■)** before calcination**,** (▲) after calcination.

Table 4.3 The apparent rate constant (k_{app}) for the photocatalytic degradation of methylene blue using synthesized ZnO before and after calcination as photocatalyst.

Catalyst	Pseudo first-order model	
	k_{app} (min^{-1})	R^2
ZnO before calcined	0.0209	0.9478
ZnO after calcined at 500°C	0.0239	0.9887

According to the above results, it can be concluded that calcination can affect on the photocatalytic activity of the synthesized ZnO justifying by the absence of carbon with higher efficiency in photodegradation of methylene blue. Although the ZnO product before calcination has smaller particle size and larger surface area, it has lower photocatalytic activity because carbon in the product blocks the light away to catalyst. Consequently, the catalyst could not adsorb the light leading to the inhibition of electron-hole pair generation, resulting in the absence of hydroxyl radical which is highly oxidative to degrade the dye pollutant. As a result, carbon content in the ZnO products shows more significantly influence on the photocatalytic activity than particles size and specific surface area in this experiment.

4.2.2 Effect of Particles Size

Another synthesis parameter which should affect the photocatalytic degradation of methylene blue is the particles size of the ZnO products. As described in section 4.1.3, the particles size of the ZnO products is increased in proportion to arc current varied from 20A to 60A. It has been reported that large specific surface area is helpful to the improvement efficiency of catalyst for photodegradation of organic pollutant [44]. In consequence, the effects of particle size on specific surface area including photocatalytic activity of the synthesized ZnO will be investigated in this part.

Particle size and specific surface areas evaluated from BET method of the synthesized ZnO at different arc currents are represented in Table 4.4. According to BET analysis, the specific surface area is decreased when the particles size is increased and no significantly different of average pore diameter was observed. Reduction in specific surface area is ascribed to the lower surface to volume ratio of the larger particles.

Table 4.4 Particle size and surface area of ZnO synthesized at different arc current.

Arc current (A)	Particle size, (nm)	Specific surface area, S_{BET}, (m^2/g)	Average pore diameter (nm)
20	33.58	11.61	5.52
30	42.64	11.11	5.44
40	48.21	10.72	5.56
50	53.54	10.55	5.34
60	59.05	10.49	5.87

The comparative photocatalytic degradation of methylene blue and the first-order linear transforms plot of the photocatalytic degradation for synthesized ZnO which is synthesized at different arc currents are shown in Figure 4.25 and 4.26, respectively. It can be seen that methylene blue can be entirely degraded within 180 min by ZnO particles synthesized at 20A, 30A and 40A while the synthesized ZnO at 50A and 60A took 240 min. Moreover, the results of the apparent rate constant calculation from pseudo first-order model presenting in Table 4.5 indicate that the photocatalytic activity of the synthesized ZnO is decrease with the increase in particle size. This is attributed to the number of surface sites available for charge transfer is subsequently decreased and led to abate the photodegradation of methylene blue. As a result, the smaller ZnO particles synthesized at low arc current is more efficient in photocatalysis than that of synthesized at high arc current.

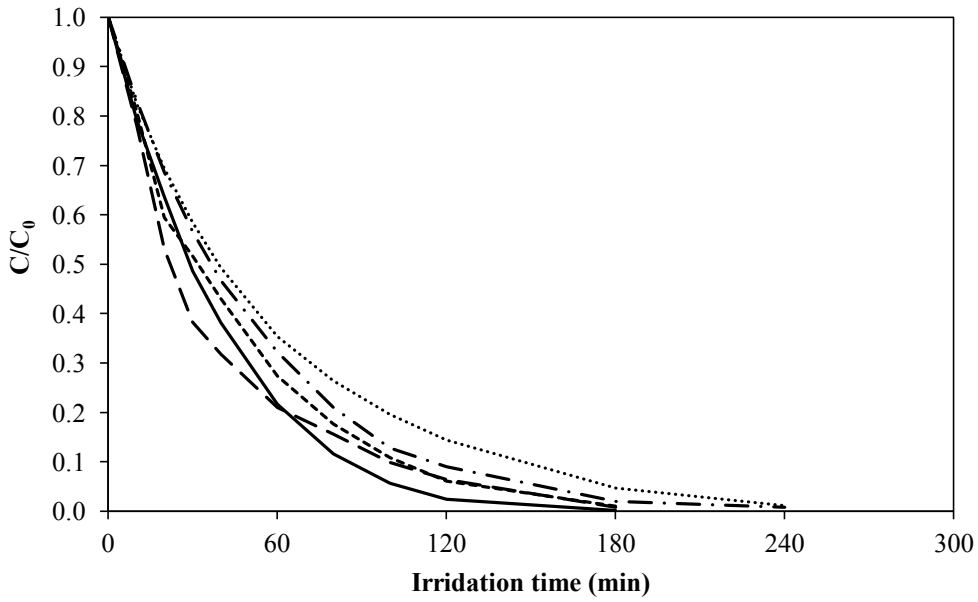

Figure 4.25 Photodegradation of methylene blue as a function of irradiation time in presence of ZnO nanoparticles prepared at various arc currents: (——) 20A, (– – -) 30A, (·····) 40A, (– · –) 50A and (·····) 60A.

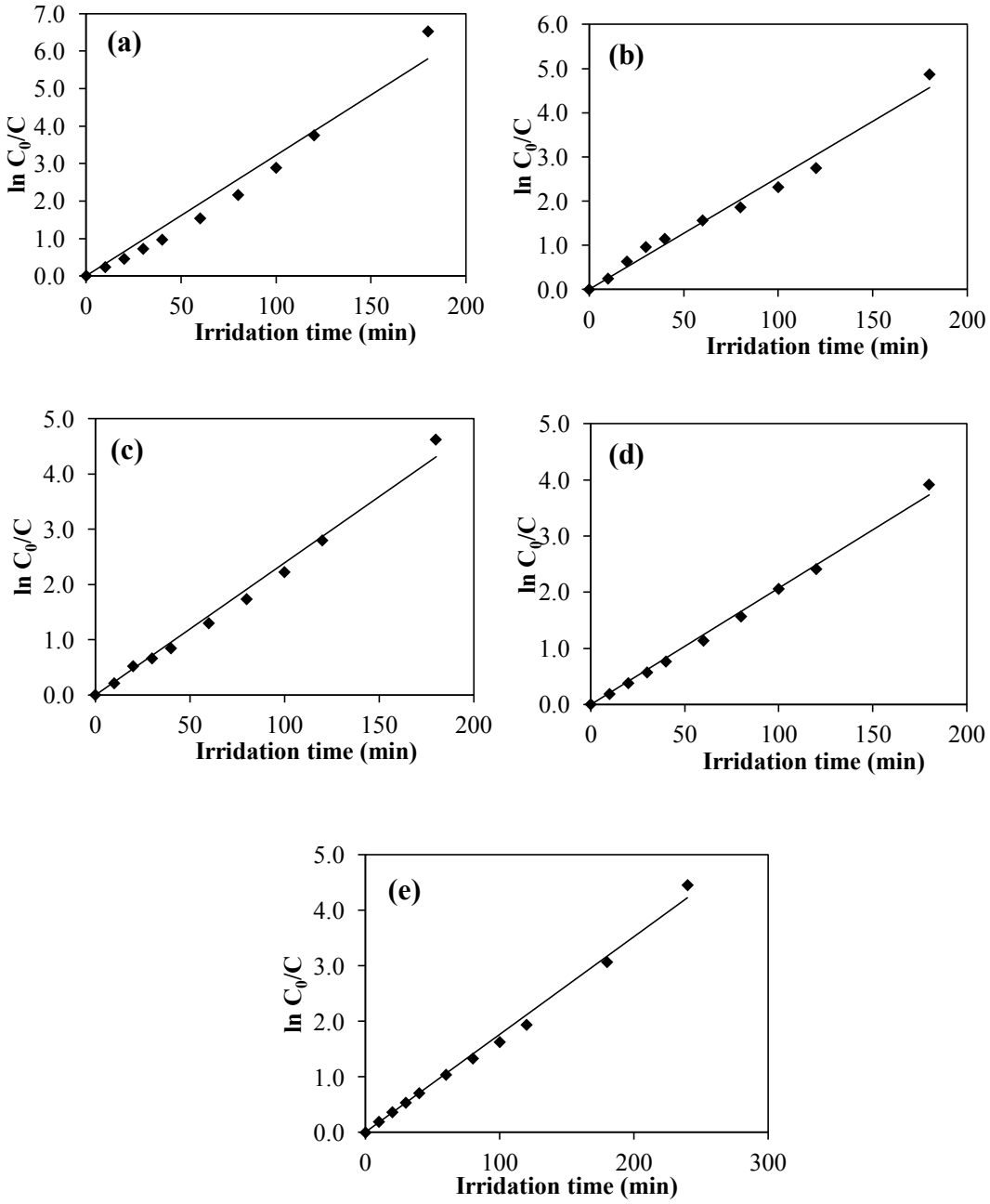

Figure 4.26 First-order linear transforms plot of the photocatalytic degradation on the Synthesized ZnO: (a) 20A**,** (b) 30A, (c) 40A, (d) 50A and (e) 60A.

Table 4.5 The apparent rate constant (k_{app}) for the photocatalytic degradation of methylene blue using synthesized ZnO at different arc current as photocatalyst.

Arc current (A)	Pseudo first-order model	
	k_{app} (min^{-1})	R^2
20	0.0322	0.9673
30	0.0254	0.9821
40	0.0239	0.9887
50	0.0208	0.9948
60	0.0176	0.9936

4.2.3 Effect of Interstitial Zn Defect

To improve the photocatalytic activity of the products, it is important to control the recombination dynamics of the photogenerated charge carriers which are electron (e^-) and hole (h^+). It has been report that not only the particle size and surface area affect on their photocatalytic performance but also an available of defect state which plays an important role in retarding the recombination of these charge carriers. For further investigation, the effect of interstitial Zn defect on the photocatalytic activity of the synthesized ZnO was studied due to the apparent of interstitial Zn defect from the synthesis condition at various oxygen concentrations in gas flow rate as report in section 4.1.6. The comparison of photocatalytic degradation of methylene blue and the first-order linear transforms plot of the photocatalytic degradation for synthesized ZnO synthesized by varying oxygen concentrations at 50%, 58.33%, 66.67% and 100% are shown in Figure 4.27 and 4.28, respectively.

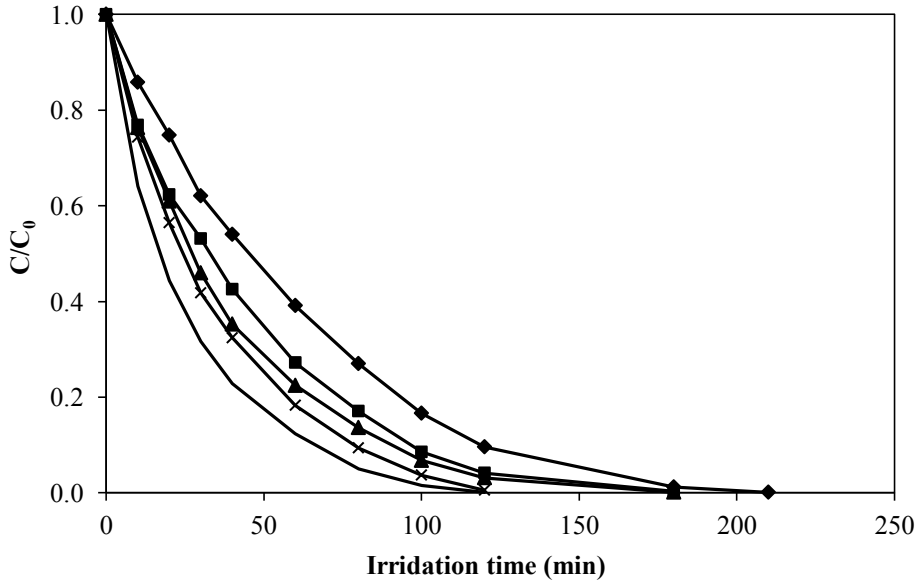

Figure 4.27 Photodegradation of methylene blue as a function of irradiation time in presence of ZnO nanoparticles prepared at various oxygen concentration: (-◆-) 50%O_2, (-■-) 58.33%O_2, (-▲-) 66.67%O_2, (-×-) 75%O_2 and (—) 100%O_2.

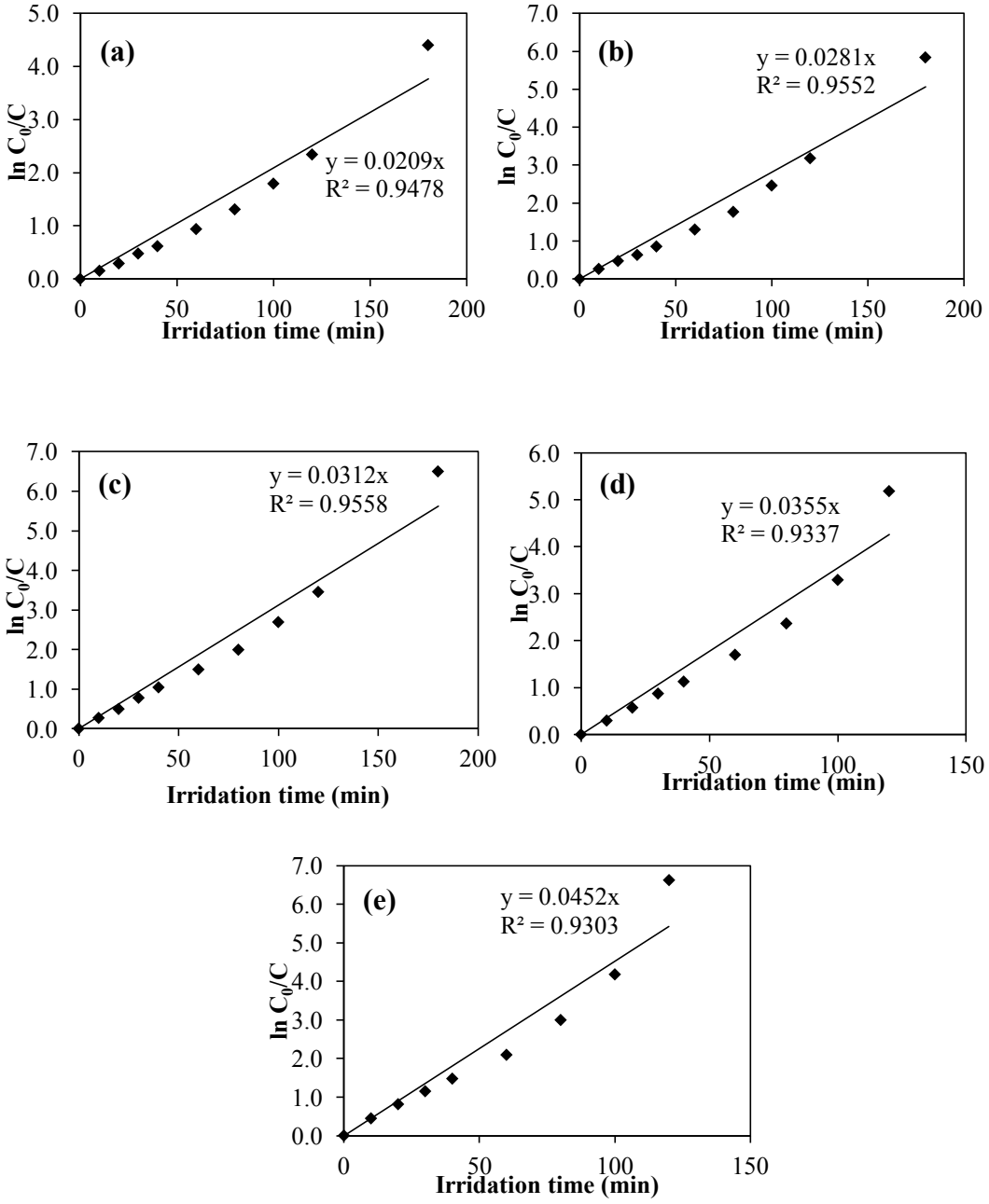

Figure 4.28 First-order linear transforms plot of the photocatalytic degradation on the Synthesized ZnO: (a) 50% O_2**,** (b) 58.33% O_2, (c) 66.67% O_2, (d) 75% O_2 and (e) 100% O_2.

It can be seen that ZnO which is synthesized using 100% O_2 at 40A possessed the highest performance for photodegradation of methylene blue which is completely eliminated within 120 min. Moreover, the results of the apparent rate constant calculation from pseudo first-order model are presented in Table 4.6. It is suggested that ZnO synthesized with 100% O_2 is the most efficient according to the highest value of apparent rate constant.

To explain the effect of defect surface on photocatalytic activity of the ZnO products, oxygen vacancy defect on ZnO surfaces is most discussed relating to its photocatalytic activity [39, 45]. On the other hand, the role of interstitial Zn according to its ability to enhance the photocatalytic activity of ZnO is barely proposed. It was reported that oxygen vacancy may act as electron capturing center which retards the recombination of charge carriers and leads to an enhanced photocatalytic activity of the photocatalysts [45].

In this study, it could be suggested that the appearance of interstitial Zn defect state on surface of ZnO can also be able to work as electron acceptors and trap the photogenerated electrons temporarily to reduce the surface recombination of electrons and holes. When the amount of the defects exceeded the optimum value they would act as the recombination centers for the photo induced electrons and holes which is unfavorable to the photocatalytic performance. Therefore, appropriate content of interstitial Zn will improve the photocatalytic performance of products.

Table 4.6 The apparent rate constant (k_{app}) for the photocatalytic degradation of methylene blue using synthesized ZnO with various oxygen concentrations as photocatalyst.

Oxygen concentration (%)	Pseudo first-order model	
	k_{app} (min^{-1})	R^2
50.00	0.0209	0.9478
58.33	0.0281	0.9552
66.67	0.0312	0.9558
75.00	0.0355	0.9337
100.00	0.0452	0.9303

CHAPTER V

CONCLUSION AND RECOMMENDATION

5.1 Summary of the Results

5.1.1Synthesis of ZnO Nanoparticles by Arc Discharge Process

1. ZnO nanoparticles can be prepared by an inexpensive and one-step procedure via a high current electrical arc discharge in water.

2. The anode speed using during operation has influence on the production of pure ZnO products. In this work, the optimum value of anode speed which can provide pure ZnO is 1.2 mm/s.

3. Arc current supplied from the direct current (DC) power supply affects the reaction. Low arc current can generate more continuous reaction than high arc current.

4. The morphology and particles size of ZnO product is depend on arc current and flow rate of carrier gas. An increasing of arc current is leading to produce more amounts of spherical shape and larger particles sizes of the products are observed. On the other hand, increasing of gas flow rate leads to reduce size of the particles.

5. Yield of product is depended on arc current, gas flow rate and water temperature. The optimum value that promote the highest yield of ZnO products are 30A of arc current and 6 L/min of gas flow rate. While, the yield of product is relatively increase with respect to water temperature.

6. Interstitial Zn defect could be obtained from the diffusion of Zn-rich atoms to ZnO lattice by the varying of oxygen concentration in the gas supply.

5.1.2Photocatalytic Activity of the Synthesized ZnO Nanoparticles

The factor which can affect the photocatalytic efficiency of the produced ZnO is calcination, particles size and defect in the surface of the ZnO product. The investigation on photocatalytic activity of ZnO suggest that the absence of carbon content after calcination, small particles size and interstitial Zn defect found in ZnO surface can give high efficiency in photodegradation of methylene blue.

5.2 Conclusions

ZnO nanoparticles were synthesized by an inexpensive and one-step procedure via a high current electrical arc discharge in water. Anode speed, arc current, flow rate and water temperature are important factor affecting morphology and size distribution of the ZnO products. Optical band gap energy of the synthesized ZnO was found to decrease relatively to Zn interstitial from the varying of oxygen concentration for arc discharge. Furthermore, photodegradation of methylene blue revealed that not only carbon content and particles size but also defect surface of the product can affect the photocatalytic activity of the produced ZnO. The optimum parameter which gives the highest photocatalytic activity of ZnO is synthesis condition using 100% O_2.

5.3 Recommendations for Future Work

1. Use Zn material for cathode instead of graphite rod to prevent impurity in the ZnO product.

2. The synthesis system should have the suction line for collecting the product lost in atmosphere and raise water level as well as reduce the level of cathode in order to increase yield of the ZnO product.

3. The effect of arc current and flow rate on the formation of interstitial Zn should be studied.

4. The others application for study the effect of interstitial Zn defect on ZnO surface should be also investigated.

REFERENCES

[1] Fan Z. and Lu J. G., Zinc Oxide Nanostructures Synthesis and Properties. (2005).

[2] Liu H. L. and Yang T.C.K., Photocatalytic inactivation of Escherichia coli and Lactobacillus helveticus by ZnO and TiO2 activated with ultraviolet light. Process Biochemistry 39,4(2003) : 475-481.

[3] Hariharan C., Photocatalytic degradation of organic contaminants in water by ZnO nanoparticles: Revisited. Applied Catalysis A: General 304 (2006) : 55-61.

[4] Shinde S. S., Shinde P. S., Bhosale C. H. and Rajpure K. Y., Zinc oxide mediated heterogeneous photocatalytic degradation of organic species under solar radiation. Photochemistry and Photobiology B: Biology 104,3(2011) : 425-433.

[5] Khodjaa A. A., Sehilia T., Pilichowski J. F. and Boule P., Photocatalytic degradation of 2-phenylphenol on TiO_2 and ZnO in aqueous suspensions. Photochemistry and Photobiology A 141(2001) : 231-239.

[6] Cheng J. P., Liao Z. M., Shi D., Liu F. and Zhang X. B., Oriented ZnO nanoplates on Al substrate by solution growth technique. Alloys and Compounds 480,2(2009) : 741-746.

[7] Mohamed R. M., Al-Rayyani M. A., Baeissa E. S. and Mkhalid I., Nano-sized Fe-metal catalyst on ZnO–SiO_2: (photo-assisted deposition and impregnation) Synthesis routes and nanostructure characterization. Alloys and Compounds 509(2011) : 6824-6828.

[8] Fu D., Han G., Chang Y. and Dong J., The synthesis and properties of ZnO–graphene nano hybrid for photodegradation of organic pollutant in water. Materials Chemistry and Physics 132,2-3(2012) : 673-681.

[9] Liu F., Cao, P. J., Zhang H. R., Li J. Q. and Gao H. J., Controlled self-assembled nanoaeroplanes, nanocombs, and tetrapod-like networks of zinc oxide. Nanotechnology 15,8(2004) : 949-952.

[10] Ashkarran A. A., Iraji Z. A., Mahdavi S. M. and Ahadian M. M., Photocatalytic activity of ZnO nanoparticles prepared via submerged arc discharge method. Applied Physics A 100,4(2010) : 1097-1102.

[11] Ashkarran A. A., Iraji Z. A., Mahdavi S. M. and Ahadian M. M., ZnO nanoparticles prepared by electrical arc discharge method in water. Materials Chemistry and Physics 118,1(2009) : 6-8.

[12] Morkoç H. and Özg€ur Ü., General Properties of ZnO. (2009).

[13] Yang H. Y., et al., Controlled Growth of ZnO nanowires and their optical properties. Advance Functional Material 12(2002) : 323-331.

[14] Wang Z.L., Zinc oxide nanostructures: growth, properties and applications. Journal of Physics: Condensed Matter 16,25(2004) : R829-R858.

[15] O'Brien S., et al., Zinc oxide thin films: Characterization and potential applications. Thin Solid Films 518,16(2010) : 4515-4519.

[16] Lupan O., et al., Synthesis of nanostructured Al-doped zinc oxide films on Si for solar cells applications. Solar Energy Materials and Solar Cells 93,8(2009) : 1417-1422.

[17] Jagadish C. and Coleman V. A., Basic Properties and Applications of ZnO, in Department of Electronic Materials Engineering, Research School of Physical Sciences and Engineering, The Australian National University: Australia.

[18] Özg r ., A comprehensive review of ZnO materials and devices. Applied Physics 98,4(2005) : 041301.

[19] Schmidt-Mende L. and MacManus-Driscoll J. L., ZnO – nanostructures, defects, and devices. Materials Today 10,5(2007) : 40-48.

[20] Janotti A. and Van de Walle C. G., Fundamentals of zinc oxide as a semiconductor. Reports on Progress in Physics 72,12(2009) : 126501.

[21] Liao Z. M., et al., Surface effects on photoluminescence of single ZnO nanowires. Physics Letters A 372,24(2008) : 4505-4509.

[22] Roychowdhury A., et al., Magnetically addressable fluorescent Fe_3O_4/ZnO nanocomposites: Structural, optical and magnetization studies. Physics and Chemistry of Solids 74,6(2013) : 811-818.

[23] Cui S., et al., Investigation on preparation of multiwalled carbon nanotubes by DC arc discharge under N_2 atmosphere. Carbon 42,5-6(2004) : 931-939.

[24] He D., et al., The effect of electric current on the synthesis of single-walled carbon nanotubes by temperature controlled arc discharge. Diamond and Related Materials 16,9(2007) : 1722-1726.

[25] Sano N., Low-cost synthesis of single-walled carbon nanohorns using the arc in water method with gas injection. Physics D: Applied Physics 37,8(2004) : L17-L20.

[26] Xing G., Jia S. l., and Shi Z. Q., The production of carbon nano-materials by arc discharge under water or liquid nitrogen. New Carbon Materials 22,4(2007) : 337-341.

[27] Ashkarran A.A., A novel method for synthesis of colloidal silver nanoparticles by arc discharge in liquid. Current Applied Physics 10,6(2010) : 1442-1447.

[28] Lunga J. K., et al., Preparation of gold nanoparticles by arc discharge in water. Alloys and Compounds (2007) : 655–658.

[29] Ashkarran A.A., Iraji Z. A., Mahdavi S. M. and Ahadian M. M., Synthesis and photocatalytic activity of WO_3 nanoparticles prepared by the arc discharge method in deionized water. Nanotechnology 19,19(2008) : 195709.

[30] Poonjarernsilp C., et al., Single-step synthesis and characterization of single-walled carbon nanohorns hybridized with Pd nanoparticles using N_2 gas-injected arc-in-water method. Carbon 49,14(2011) : 4920-4927.

[31] Li N., Wang Z., and Shi Z., Synthesis of Graphenes with Arc-Discharge Method. Physics and Applications of Graphene: 23-36.

[32] Wang H., et al., Large-scale synthesis of single-walled carbon nanohorns by submerged arc. Nanotechnology 15,5(2004) : 546-550.

[33] Sano N., Akita Y., and Tamon H., Effects of synthesis conditions on the structural features and methane adsorption properties of single-walled carbon nanohorns prepared by a gas-injected arc-in-water method. Applied Physics 109,12(2011) : 124305.

[34] Poonjarernsilp C., et al., A model of reaction field in gas-injected arc-in-water method to synthesize single-walled carbon nanohorns: Influence of water temperature. Applied Physics 106,10(2009) : 104315.

[35] Zou L., et al., Removal of VOCs by photocatalysis process using adsorption enhanced TiO_2–SiO_2 catalyst. Chemical Engineering and Processing: Process Intensification 45,11(2006) : 959-964.

[36] Philippopoulos C. J. and Nikolaki M. D., Photocatalytic processes on the oxidation of organic compounds in water, New Trends in Technologies : 89-107.

[37] Mai F.D., et al., Photodegradation of methyl green using visible irradiation in ZnO suspensions. Chromatography A 1189,1-2(2008) : 355-365.

[38] Elmolla E. S. and Chaudhuri M., Degradation of amoxicillin, ampicillin and cloxacillin antibiotics in aqueous solution by the UV/ZnO photocatalytic process. Hazardous Materials 173,1-3(2010) : 445-449.

[39] Wang Y., et al., Controllable synthesis of ZnO nanoflowers and their morphology-dependent photocatalytic activities. Separation and Purification Technology 62,3(2008) : 727-732.

[40] Lei A., et al., Facile synthesis and enhanced photocatalytic activity of hierarchical porous ZnO microspheres. Materials Letters 66,1(2012) : 72-75.

[41] Mekasuwandumronga O., et al., Effects of synthesis conditions and annealing post-treatment on the photocatalytic activities of ZnO nanoparticles in the degradation of methylene blue dye. Chemical Engineering 164 (2010) : 77-84.

[42] Sano N., et al., Influence of arc duration time on the synthesis of carbon nanohorns by a gas-injected arc-in-water system: application to polymer electrolyte fuel cell electrodes. Plasma Sources Science and Technology 20,3(2011) : 034002.

[43] Roy M., Mali K., Joshi N., Misra D. S. and Kulshreshtha S. K., Deposition of hydrogenated amorphous carbon films with enhanced sp_3-C bonding on nanocrystalline palladium interlayer. Diamond and Related Materials 16,3(2007) : 517-525.

[44] Han J., et al., Comparative photocatalytic degradation of estrone in water by ZnO and TiO_2 under artificial UVA and solar irradiation. Chemical Engineering Journal 213(2012) : 150-162.

[45] Wang H. and Xie C., The effects of oxygen partial pressure on the microstructures and photocatalytic property of ZnO nanoparticles. Physica E: Low-dimensional Systems and Nanostructures 40,8(2008) : 2724-2729.

APPENDICES

APPENDIX A

CALCULATION OF THE CRYSTALLITE SIZE

Calculation of the crystallite size by Debye-Scherrer equation

The crystallite size was calculated from the half-height width of the diffraction peak of XRD pattern using the Debye-Scherrer equation as shown in A.1.

$$D = \frac{k\lambda}{\beta \cos\theta} \qquad \text{(A.1)}$$

Where D = Crystallite size, Å

k = Crystallite-shape factor = 0.9

λ = X-ray wavelength, 1.5406 Å for CuKα

Θ = Observed peak angle, degree

β = X-ray diffraction broadening, radian

Example: Calculation of the crystallite size of zinc oxide

The half-height width of 101 diffraction peak = 0.311 (from Figure A.1)

$= \left(\frac{2\pi}{360}\right) \times 0.311$

= 0.00543 radian

Thus, β = 0.00543 radian

2Θ = 36.18

Θ = 18.09

λ = 1.5406 Å

The crystallite size $= \frac{0.9 \times 1.5406}{0.00543 \cos(18.09)}$ = 352.17 Å = 35.22 nm

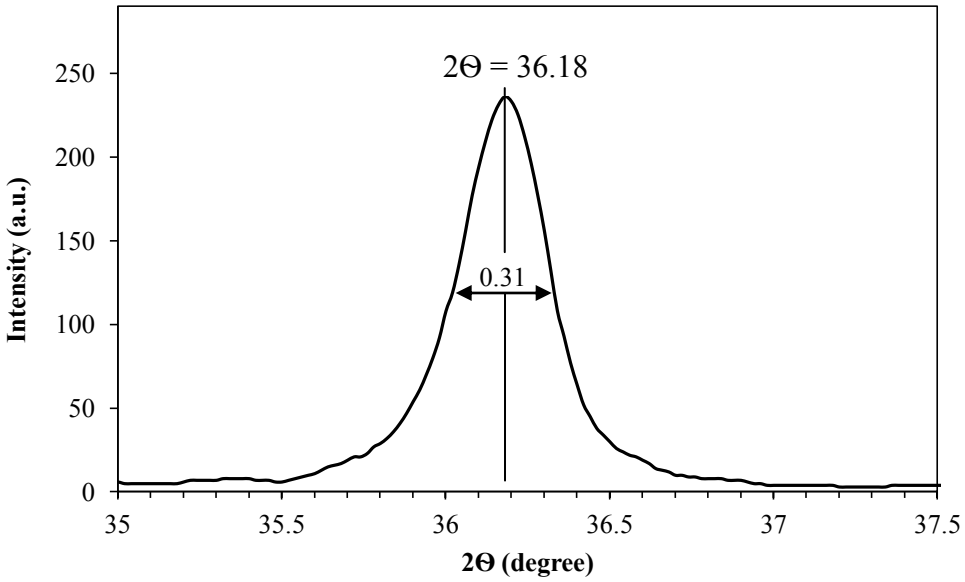

Figure A.1 The observation peak of zinc oxide for calculating the crystallite size.

APPENDIX B

CALCULATION OF PERCENTAGE OF ZINC SOLID

The percentage of Zn solid which could describe continuity of the reaction can be calculated by using Eq. B.1.

$$\%\text{Weight of Zn solid} = \frac{\text{Wt.of Zn solid at bottom}}{\text{Consume wt.of Zn anode}} \times 100 \qquad \text{(B.1)}$$

Where

Consume wt. of Zn anode = wt. of Zn anode before arc discharge - wt. of Zn anode after arc discharge

Example: Calculation of the percentage of Zn solid by using 20A arc current

Weight of Zn anode before arc discharge	=	4.3650 g
Weight of Zn anode after arc discharge	=	1.6760 g
Weight of Zn solid at bottom	=	1.0518 g

$$\%\text{Weight of Zn solid} = \frac{1.0518}{4.3650 - 1.6760} \times 100 = 39.11\%$$

APPENDIX C

CALCULATION OF THE BAND GAP ENERGY

For the evaluation of band gap energy of photocatalyst UV-VIS spectrophotometry equipped with diffuse reflectance accessory. The determination of band gap is followed by the Tauc plot method.

The following relational expression proposed by Tauc, Davis, and Mott is used as shown in Eq. B.1.

$$(h\nu\alpha)^{(1/n)} = A(h\nu - E_g) \quad \text{(C.1)}$$

Where, h = Planck's constant, 6.626×10^{-34} m^2 kg / s

υ = frequency of vibration

α = absorption coefficient

A = proportional constant

E_g = band gap, eV

The value of the exponent n denotes the nature of the sample transition, for direct allowed transition n = ½.

The acquired diffuse reflectance spectrum is converted to Kubelka-Munk function. Thus, the vertical axis is converted to quantity $F(R_\infty)$, which is proportional to the absorption coefficient. The α in the Tauc equation is substituted with $F(R_\infty)$. Thus, in the actual experiment, the relational expression becomes Eq. B.2.

$$(h\nu F(R_\infty))^2 = A(h\nu - E_g) \quad \text{(C.2)}$$

Where

$$R_\infty = \frac{R_{sample}}{R_{s\,\tan dard}} \quad \text{(C.3)}$$

Using the Kubelka-Munk function, the $(h\nu F(R_\infty))^2$ was plotted against hν. The curve plots the value of hν on the horizontal axis and $(h\nu F(R_\infty))^2$vertical axis and the respective tangent are depicted. The value associated with the point of intersection of the line tangent to the plotted curve inflection point with the horizontal axis (hν axis) becomes the band gap Eg value. The calculated data and the curve of $(h\nu - (h\nu F(R_\infty))^2$ are represented in Table C.1 and Figure C.1, respectively.

Table C.1 Calculated data from Kubelka-Munk function.

Band energy		$R_{standard}$	Sample			
Joules	eV		%R	R_∞	$f(R_\infty)$	$[f(R_\infty)h\nu]^2$
5.6E-19	3.497	99.649	18.024	0.181	1.855	42.067
5.59E-19	3.487	99.850	18.109	0.181	1.848	41.513
5.57E-19	3.477	99.872	18.080	0.181	1.852	41.497
5.56E-19	3.468	99.648	18.143	0.182	1.837	40.590
5.54E-19	3.458	99.660	18.175	0.182	1.833	40.169
5.53E-19	3.448	99.797	18.270	0.183	1.823	39.510
5.51E-19	3.439	99.623	18.294	0.184	1.815	38.942
5.49E-19	3.429	99.801	18.368	0.184	1.809	38.475
5.48E-19	3.420	99.729	18.415	0.185	1.800	37.898
5.46E-19	3.411	99.516	18.465	0.186	1.787	37.164
5.45E-19	3.401	99.915	18.468	0.185	1.797	37.376
5.43E-19	3.392	99.836	18.535	0.186	1.786	36.699
5.42E-19	3.383	99.999	18.640	0.186	1.776	36.072
5.4E-19	3.373	99.629	18.724	0.188	1.754	35.026
5.39E-19	3.364	99.885	18.856	0.189	1.743	34.390
5.38E-19	3.355	99.692	18.921	0.190	1.729	33.665
5.36E-19	3.346	99.697	19.093	0.192	1.707	32.613
5.35E-19	3.337	99.894	19.268	0.193	1.689	31.756
5.33E-19	3.328	99.787	19.496	0.195	1.657	30.408
5.32E-19	3.319	99.824	19.845	0.199	1.614	28.719
5.3E-19	3.310	99.777	20.259	0.203	1.564	26.810
5.29E-19	3.302	99.798	21.008	0.211	1.480	23.894
5.28E-19	3.293	99.699	21.936	0.220	1.383	20.727
5.26E-19	3.284	99.657	23.111	0.232	1.272	17.452
5.25E-19	3.276	99.846	24.343	0.244	1.173	14.756
5.23E-19	3.267	99.910	25.873	0.259	1.060	11.997
5.22E-19	3.258	99.684	27.484	0.276	0.951	9.609
5.21E-19	3.250	99.768	29.266	0.293	0.851	7.651
5.19E-19	3.241	99.883	31.141	0.312	0.760	6.063
5.18E-19	3.233	99.749	33.059	0.331	0.674	4.753
5.17E-19	3.225	99.699	34.847	0.350	0.605	3.809

Table C.1 (Continued) Calculated data from Kubelka-Munk function.

Energy		$R_{standard}$	Sample			
joules	eV		%R	R_∞	$f(R_\infty)$	$[f(R_\infty)hv]^2$
5.15E-19	3.216	99.765	36.585	0.367	0.547	3.093
5.14E-19	3.208	99.665	38.261	0.384	0.494	2.515
5.13E-19	3.200	99.891	39.720	0.398	0.456	2.131
5.11E-19	3.191	99.607	40.968	0.411	0.421	1.808
5.1E-19	3.183	99.687	42.144	0.423	0.394	1.574
5.09E-19	3.175	99.906	43.204	0.432	0.372	1.398
5.07E-19	3.167	99.753	44.100	0.442	0.352	1.243
5.06E-19	3.159	99.673	44.909	0.451	0.335	1.120
5.05E-19	3.151	99.892	45.745	0.458	0.321	1.022
5.04E-19	3.143	99.746	46.303	0.464	0.309	0.944
5.02E-19	3.135	99.806	46.982	0.471	0.298	0.870
5.01E-19	3.127	99.774	47.466	0.476	0.289	0.816
5E-19	3.119	99.876	47.908	0.480	0.282	0.775
4.98E-19	3.111	99.675	48.417	0.486	0.272	0.717
4.97E-19	3.104	99.780	48.768	0.489	0.267	0.689

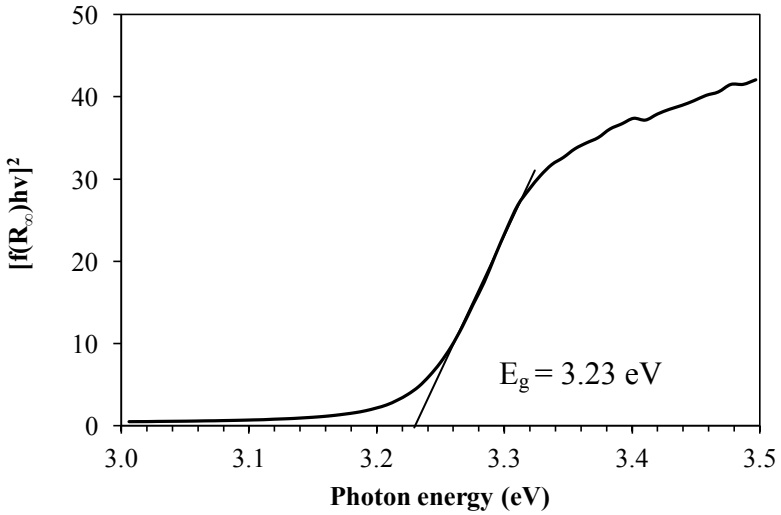

Figure C.1 Kubelka-Munk transformed reflectance spectra of the synthesized zinc oxide.

APPENDIX D

METHYLENE BLUE CALIBRATION CURVE

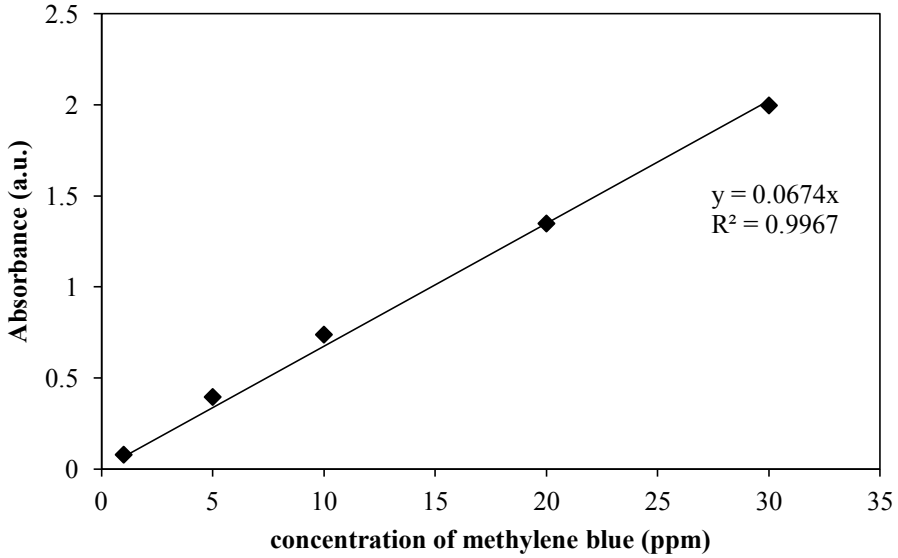

Figure D.1 The calibration curve of methylene blue**.**

APPENDIX E

LIST OF PUBLICATIONS

1. Chortip Termpornvithit and Varong Pavarajarn "Synthesis and photocatalytic activity of ZnO nanoparticles via arc discharge in water" Proceedings of the Pure and Applied Chemistry International 2013, Bangsaen Beach, Thailand, January 23 – 25, 2013.
2. Chortip Termpornvithit and Varong Pavarajarn "Photocatalytic Activity of ZnO Nanoparticles synthesized by Arc Discharge in Water" Proceedings of the Joint Conference on Renewable Energy and Nanotechnology 2013, Hiroshima, Japan, November 25 – 26, 2013.

VITA

Miss Chortip Termpornvithit was born on August 6, 1988 in Chaingrai Province, Thailand. In 2011, she graduated the Bachelor Degree of Chemical Technology from Faculty of Science, Chulalongkorn University. After that, she continued her Master's study at Chulalongkorn University in Center of Excellence in Particle Technology at Chemical Engineering Department, Faculty of Engineering in June, 2011.